Anisotropic scattering of electrons by N_2 and its effect on electron transport

A. V. Phelps*
Joint Institute for Laboratory Astrophysics, National Bureau of Standards and University of Colorado, Boulder, Colorado 80309

L. C. Pitchford†
Sandia National Laboratories, Albuquerque, New Mexico 87185

(Received 22 October 1984)

As part of a systematic study of approximations commonly made in solutions of the Boltzmann equation for electrons in molecular gases, we have investigated the effects of anisotropic scattering on electron transport coefficients in N_2 and have extended our study of the multiterm expansion technique to higher E/n. A critical survey of published data yields a set of differential and integral cross sections for electron energies from 0.003 to 10^4 eV. For electric-field—to—gas-density ratios E/n between 10 and 500 Td (1 Td$=10^{-21}$ V m^2), the changes in the commonly measured transport and reaction coefficients resulting from the introduction of anisotropic elastic and inelastic scattering, while keeping the elastic momentum-transfer cross section constant, are less than 1%. These calculations were made with use of the multiterm spherical-harmonic expansion solution of the Boltzmann equation. For $500 < E/n < 1500$ Td the changes in scattering anisotropy cause changes in transport and reaction coefficients which increase with E/n to about 10%. The errors in drift velocity, mean energy, and the reaction coefficients resulting from the use of the two-term spherical-harmonic expansion rather than a six-term expansion are less than 3% at 1500 Td. However, the errors in the diffusion coefficients become large ($>25\%$) at our highest E/n. The calculated transport coefficients are in generally good agreement with experiment for E/n less than 300 Td, but the differences increase at higher E/n. The importance of proper interpretation of ionization and excitation experiments at high E/n is illustrated by calculations which model either an exponential growth of density in time or an exponential growth with position. The calculated ionization coefficients are low compared to most experiments for E/n less than 200 Td. At $E/n > 600$ Td the agreement is good for the spatial growth experiments, but the calculated values are below experiment from the temporal growth experiments. The calculated excitation coefficients are generally higher than experiment at low and high E/n but in agreement with experiment at E/n near 150 Td.

I. INTRODUCTION

The availability of differential scattering data for electrons in N_2 and the development of the multiterm spherical-harmonic expansion techniques for solution of the electron Boltzmann equation[1] make possible this investigation of the effects of anisotropic scattering on electron transport in N_2. The present work is part of a systematic study[1–3] of the effects of various simplifying approximations on the solutions of the Boltzmann equation for electrons in molecular gases, such as N_2. Our primary objective has been to develop and test techniques for improving the accuracy of the calculated values of measured transport and reaction-rate coefficients. Although this series of papers has included some changes in electron collision cross sections which improve the agreement between calculations and experiment, we are much more concerned with the effects of the computational techniques, secondary-electron distributions, and angular distribution on these calculated transport coefficients. The initial paper,[1] which we will refer to as I, describes techniques for adding higher-degree spherical harmonics (Legendre polynomials) to the two-term or Lorentz approximation when solving the electron Boltzmann equation. This work demonstrated the changes in calculated transport and reaction coefficients which occur when the inelastic cross section becomes comparable with the elastic momentum-transfer cross section, as in N_2 at energies near 2 eV. In the second paper,[2] which will be referred to as II, we showed that at low E/n in N_2 the use of the two-term approximation causes large errors in the calculation of excitation rate coefficients, but that for low and moderate E/n the errors in transport coefficients are generally small, e.g., less than 8%. More recently[3] in paper III, we examined the effects of various approximations to the distribution in energy of secondary electrons produced in the process of electron-impact ionization. We found that the primary consideration is to include the new electron in the Boltzmann equation. The results are sufficiently insensitive to the details of the assumed secondary-electron energy distribution so as to allow the use of delta function secondary-electron energy distributions adjusted to satisfy energy and momentum conservation.

The question of the effects of anisotropic scattering on solutions of the Boltzmann equation and on electron

transport calculations has been considered for moderate E/n and electron energies and for some model angular distributions.[4,5] These calculations show that for realistic angular distributions the errors in the calculated transport coefficients are small, i.e., less than 5%. In a preliminary report on the present work[6] we assembled a set of anisotropic cross sections for electrons in N_2 and applied it to the calculation of electron-energy distribution functions and transport coefficients at moderate E/n. In the present paper we discuss these cross sections and extend their application to higher electron energies and higher E/n. At moderate E/n and mean energies, we find that the calculated effects of anisotropic scattering are small enough so as to be observed only in precision swarm experiments. At higher E/n and higher electron energies where electron scattering is known to be highly anisotropic, we find increasingly important errors in the solutions of the electron Boltzmann equation obtained using the usual assumptions of momentum-transfer elastic scattering and isotropic inelastic scattering. We will limit E/n to 3000 Td and below, since experiments[7] and recent theory[8] for N_2 indicate the onset of departures from the hydrodynamic model, e.g., the spatial growth constant α_i varies with position,[7] at E/n between 1500 and 3000 Td. We will designate the departures from the hydrodynamic model at high values of E/n as runaway effects since energetic electrons gain more energy from the electric field than they lose in collisions. Kücükarpaci and Lucas[9] and Kunhardt and Tzeng[9] have investigated the effects of anisotropic scattering on electron motion in N_2 using Monte Carlo techniques. We will discuss these results in Sec. IV.

A brief review of the techniques used to solve the electron Boltzmann equation is given in Sec. II. Then our choice of an anisotropic cross section set for N_2 is discussed in Sec. III. Calculated electron-energy distributions, transport coefficients, and reaction-rate coefficients are discussed in Sec. IV. Our results are compared with experimental data in Sec. V.

II. SOLUTION OF THE BOLTZMANN EQUATION

In this section we summarize the theoretical expressions necessary to define the cross sections, transport and rate coefficients, and calculational procedures used in this paper. Since the general theory of the expansions in powers of the density gradients and in spherical harmonics has been presented elsewhere,[1,2,10–12] we will discuss only enough detail to illustrate our procedures. The Boltzmann equation for the distribution function $F(\mathbf{v},\mathbf{r},\mathbf{t})$ can be written as

$$\frac{\partial F(\mathbf{v},\mathbf{r},t)}{\partial t}+\mathbf{v}\cdot\nabla_{\mathbf{r}}F+\mathbf{a}\cdot\nabla_{\mathbf{v}}F=nC[F]\ , \tag{1}$$

where $\mathbf{r}$ and $\mathbf{v}$ are the position and velocity of an element of phase space at time t, $\mathbf{a}=-|e/m|\mathbf{E}$ is the acceleration of an electron of charge e and mass m caused by the electric field $\mathbf{E}$, and $C[F]$, is the collision operator to be discussed later.

In this paper we make use of two different approaches to the treatment of the effect of the spatial dependence of the electron density on the Boltzmann equaton. The first is the density gradient expansion and is particularly appropriate to time-of-flight experiments in which quantities proportional to the time and spatially dependent electron density are measured.[13,14] To second order in the derivatives and in cylindrical coordinates, this expansion can be written as

$$\begin{aligned}F(\mathbf{v},\mathbf{r},t)=f(\mathbf{v})n_e(\mathbf{r},t)&-\frac{g_z(\mathbf{v})}{n}\frac{\partial n_e(\mathbf{r},t)}{\partial z}\\&-\frac{g_\rho(\mathbf{v})}{n}\frac{\partial n_e(\mathbf{r},t)}{\partial\rho}+\frac{h_{zz}(\mathbf{v})}{n^2}\frac{\partial^2 n_e(\mathbf{r},t)}{\partial z^2}\\&+\frac{h_{\rho\rho}(\mathbf{v})}{n^2}\frac{1}{\rho}\frac{\partial}{\partial\rho}\left[\rho\frac{\partial n_e(\mathbf{r},t)}{\partial\rho}\right]\ .\end{aligned} \tag{2}$$

Here $f(\mathbf{v})$ is the velocity distribution in the absence of density gradients, $\rho=|\mathbf{r}|\sin\phi$, ϕ is the angle of the position vector $\mathbf{r}$ with the direction of electron acceleration, $n_e(\mathbf{r},t)$ is the electron density, $g_z(\mathbf{v})$ and $g_\rho(\mathbf{v})$ are the velocity distributions associated with the gradient of the electron density in the direction of acceleration and the direction perpendicular to the acceleration, and $h_{zz}(\mathbf{v})$ and $h_{\rho\rho}(\mathbf{v})$ are the velocity distributions associated with the second derivative of the electron density in the direction of $\mathbf{a}$ and at right angles to $\mathbf{a}$. Substitution of Eq. (2) into Eq. (1) and the integration over all velocities yields the continuity equation for the electron density, i.e.,

$$\begin{aligned}\frac{\partial n_e(\mathbf{r},t)}{\partial t}=\nu n_e(\mathbf{r},t)&-W\frac{\partial n_e(\mathbf{r},t)}{\partial z}+D_L\frac{\partial^2 n_e(\mathbf{r},t)}{\partial z^2}\\&+\frac{D_T}{\rho}\frac{\partial}{\partial\rho}\left[\rho\frac{\partial n_e(\mathbf{r},t)}{\partial\rho}\right]\ ,\end{aligned} \tag{3}$$

where

$$\nu=n\int C[f(\mathbf{v})]d^3v\ , \tag{4}$$

$$W=\mu E=\int v_z f(\mathbf{v})d^3v+\int C[g_z(\mathbf{v})]d^3v\ , \tag{5}$$

$$nD_L=\int v_z g_z(\mathbf{v})d^3v+\int C[h_{zz}(\mathbf{v})]d^3v\ , \tag{6}$$

and

$$nD_T=\int v\sin\theta\, g_\rho(\mathbf{v})d^3v]+\int C[h_{\rho\rho}(\mathbf{v})]d^3v\ . \tag{7}$$

The normalization relations are

$$\int f(\mathbf{v})d^3v=1$$

and

$$\begin{aligned}\int g_z(\mathbf{v})d^3v=\int g_\rho(\mathbf{v})d^3v&=\int h_{zz}(\mathbf{v})d^3v\\&=\int h_{\rho\rho}(\mathbf{v})d^3v=0\ .\end{aligned} \tag{8}$$

Here $v_z=|\mathbf{v}|\cos\theta$ and θ is the angle of the velocity vector with respect to the direction of electron acceleration. The temporal growth constant ν, the drift velocity W, the mobility μ, the longitudinal diffusion coefficient D_L, and the transverse diffusion coefficient D_T defined by Eqs. (4)–(7) are independent of position and time in what is called the hydrodynamic approximation,[12] e.g., when the electrons have had a sufficient number of collisions so that their distribution in energy is independent of their in-

itial energy distribution. Note that the integrals over the collision operator $C[f]$ in Eqs. (4)—(7) were not present in I and II because electron production and loss were not included in the Boltzmann equation.

Equations for $f(\mathbf{v})$, $g_z(\mathbf{v})$, $g_\rho(\mathbf{v})$, $h_{zz}(\mathbf{v})$, and $h_{\rho\rho}(\mathbf{v})$ are obtained by substituting Eq. (2) into Eq. (1) and setting coefficients of $n_e(\mathbf{r},t)$ and its derivatives equal to zero. The equation for $f(\mathbf{v})$ is

$$\mathbf{a}\cdot\nabla_v f(\mathbf{v})=nC[f(\mathbf{v})]-\nu f(\mathbf{v}) . \tag{9}$$

The $\nu f(\mathbf{v})$ term accounts for the temporal growth and was added in III with the resultant requirement that Eq. (9) be solved as an eigenvalue problem. The differential equation for $g_z(\mathbf{v})$ is

$$\mathbf{a}\cdot\nabla_v g_z(\mathbf{v})=nC[g_z(\mathbf{v})]-\nu g_z(\mathbf{v})-n(W-v_z)f(\mathbf{v}) . \tag{10}$$

Integration of this equation over all velocities gives Eq. (5). The solution of Eq. (10) has been discussed by Tagashira *et al.*[11] Because of difficulties[2] encountered in the evaluation of $g_z(\mathbf{v})$ in the case of N_2, but not other gases,[1] we will not present values of D_L or of the second integral of Eq. (5). We will assume that this correction to W can be neglected in our evaluation of the effects of anisotropic scattering or of the effects of the truncation of the spherical-harmonic expansion. In this case the solution of Eq. (10) simplifies to the equations discussed in II and III. The differential equation for $g_\rho(\mathbf{v})$ is

$$\mathbf{a}\cdot\nabla_v g_\rho(\mathbf{v})=nC[g_\rho(\mathbf{v})]-\nu g_\rho(\mathbf{v})+n v\sin\theta[f(\mathbf{v})] . \tag{11}$$

As for W, we neglect the contribution of the second integral in Eq. (7) to the value of D_T.

Similar but more complicated equations are obtained[11,12] for $h_{zz}(\mathbf{v})$ and $h_{\rho\rho}(\mathbf{v})$. Since these equations were not solved for this paper, they will not be given here.

The transport and ionization coefficients of Eq. (3) are sometimes termed time-of-flight (TOF) coefficients,[11,12] since Eq. (3) is often applicable to the analysis of data obtained from time-of-flight experiments.[13,14] We prefer to call these coefficients the density gradient expansion coefficients and reserve the time-of-flight terminology for the experiments and the transport coefficients derived by fitting solutions to Eq. (3) to these experiments. This procedure is consistent with Blevin's[15] point that Eq. (3) is applicable to the analysis of data obtained from many cylindrically symmetric experiments, i.e., (a) data from time-of-flight experiments, (b) the spatial growth constant from time-integrated or steady-state (Townsend) experiments, or (c) the temporal growth constant from spatially integrated or induced-current (pulsed Townsend) experiments, provided that the conditions for the hydrodynamic model are satisfied. Thus the application of Eq. (3) to the analysis of parallel plane, steady-state ionization experiments at positions far from an electrode yields

$$n_e(z)=n_0 e^{\alpha_i z} , \tag{12}$$

where, for the number of terms in the density gradient expansion given in Eqs. (2) and (3) the spatial growth constant α_i is the root of the equation

$$\frac{\nu}{n}-\frac{\alpha_i}{n}W+\left[\frac{\alpha_i}{n}\right]^2(nD_L)=0 . \tag{13}$$

Equation (13), thus establishes the connection[13,14] between the density gradient expansion coefficients ν, W, and D_L and the spatial growth (Townsend) ionization coefficient α_i. It must be keep in mind that this approach assumes the density gradients are small enough so that the expansion given in Eq. (2) is valid, e.g., that $\alpha_i D_L \ll W$ in Eq. (13). Note that $\nu/\alpha_i \equiv V_p \approx W-\alpha_i D_L$ defines a drift velocity which can be measured in some experiments.[16] As predicted and demonstrated by Blevin *et al.*,[14,15] the presence of spatial gradients must be taken into account in the calculation of excitation coefficients for comparison with steady-state excitation experiments[17,18] when the E/n is high enough so that ionization is important.

Our second approach to the solution of the steady-state Boltzmann equation in the presence of an exponential spatial growth is to assume that the electron energy distribution can be written as

$$F(\mathbf{v},\mathbf{r},t)=f_{ss}(\mathbf{v})e^{\alpha_i z} . \tag{14}$$

Use of this form[19] instead of Eqs. (10) and (13) allows one to considerably simplify the Boltzmann calculation for steady-state experiments in which α_i is determined from the variation of $n_e(z)$ with position or with electrode spacing as in the steady-state Townsend experiment.[7,11] Thus, substitution of Eq. (14) into Eq. (1) yields

$$\mathbf{a}\cdot\nabla_v f_{ss}(\mathbf{v})+v_z\alpha_i f_{ss}(\mathbf{v})=nC[f_{ss}(\mathbf{v})] . \tag{15}$$

The spatial ionization coefficient α_i is obtained by integrating Eq. (15) over all velocities, i.e.,

$$\frac{\alpha_i}{n}=\frac{\int v Q_0^i(v) f_{ss}(\mathbf{v})d^3v}{\int v_z f_{ss}(\mathbf{v})d^3v}\equiv\frac{k_{iss}}{V_d} , \tag{16}$$

where $Q_c^i(v)$ is the total ionization cross section. Equations (15) and (16) must be solved iteratively to obtain $f_{ss}(\mathbf{v})$, α_i/n, etc. Note that the α_i/n calculated by Eq. (16) is the same as that which would be obtained by extending the density gradient expansion and Eq. (13) to an infinite number of terms. Generally, the ionization rate coefficient k_{iss} defined by the numerator of Eq. (16) is smaller than $\nu/n\equiv k_i$ at the same E/n, i.e., the diffusion of electrons toward the cathode due to the density gradient lowers the number of high-energy electrons in $f_{ss}(\mathbf{v})$ compared to those in $f(\mathbf{v})$ from Eq. (9). This difference is illustrative of the effect of density gradients on excitation and ionization coefficients discussed by Blevin.[15] The convective drift velocity V_d defined in the denominator of Eq. (16) is also lower than the corresponding velocity from the density gradient expansion V_p. This discussion shows that the calculations of α_i/n can be made using only $f_{ss}(v)$ in Eq. (16), rather than using $f(\mathbf{v})$, $g_z(\mathbf{v})$, and $h_{zz}(\mathbf{v})$ as in Eqs. (5), (6), and (13).

The similarity of Eqs. (9) and (15) leads us to define a modified collision operator $B[f(\mathbf{v})]$ and to consider the equation

$$\mathbf{a}\cdot\nabla_v f(\mathbf{v})+v_z\alpha_i f(\mathbf{v})=nB[f(\mathbf{v})] \equiv nC[f(\mathbf{v})]-\nu f(\mathbf{v}) . \tag{17}$$

We will consider only cases in which either ν or α_i is zero, although one might well analyze experiments in which it is a good approximation to assume that both ν and α_i were nonzero. Note that in Eqs. (15) and (17) the magnitude of α_i is not restricted by the requirement of rapid convergence of the density gradient expansion as in Eq. (13).

We next make use of the spherical-harmonic expansion technique for solving for the electron velocity or energy distribution. In this discussion we will consider only Eq. (17), since the extension of the method to equations such as Eqs. (10) and (11) is straightforward.[2] As in II, the velocity distribution $f(\mathbf{v})$ is written in the form

$$f(\mathbf{v})=\sum_{j=0}^{m-1} f_j(\epsilon)P_j(\cos\theta) , \tag{18}$$

where ϵ is the electron energy, m is the number of terms in the expansion, $P_j(\cos\theta)$ is the zero-order Legendre polynomial of degree j, and $f(\epsilon)$ is normalized by

$$\int_0^\infty \epsilon^{1/2} f_0(\epsilon)d\epsilon=1 . \tag{19}$$

With these assumptions Eq. (9) can be written as a series of coupled equations of the form

$$\frac{eE}{n}\frac{j}{(2j-1)}\left[\epsilon\frac{df_{j-1}}{d\epsilon}-\frac{(j-1)}{2}f_{j-1}\right]+\frac{eE}{n}\frac{(j+1)}{(2j+3)}\left[\epsilon\frac{df_{j+1}}{d\epsilon}+\frac{(j+2)}{2}f_{j+1}\right]+\epsilon\frac{\alpha_i}{n}\left[\frac{j}{(2j-1)}f_{j-1}+\frac{(j+1)}{(2j+3)}f_{j+1}\right]=B[f_j] , \tag{20}$$

where $0\le j\le m-1$ and the modified collision operator is given by

$$B[f_j(\epsilon)]=-\epsilon f_j(\epsilon)Q_T(\epsilon)+\epsilon f_j(\epsilon)Q_j^0(\epsilon)+\sum_{k=1}^{p}(\epsilon+\epsilon_k)f_j(\epsilon+\epsilon_k)Q_j^k(\epsilon+\epsilon_k)+\frac{2m}{M}\delta_{j0}\frac{d}{d\epsilon}[\epsilon^2 Q_m^0(\epsilon)f_0(\epsilon)]+\int_{2\epsilon+u_i}^{\infty} uq_{\rm sec}^i(j,u,\epsilon)f_j(u)du+\int_{\epsilon+u_i}^{2\epsilon+u_i} uq_{\rm sca}^i(j,u,\epsilon)f_j(u)du-\frac{\epsilon}{v}\frac{\nu}{n}f_j(\epsilon) . \tag{21}$$

Here $\delta_{jl}=1$ for $j=l$ and $\delta_{jl}=0$ for $j\neq l$, ϵ_k and u_i are the threshold energies for excitation and ionization, p is the number of excitation processes, and M is the mass of the gas molecule. The derivations of the various terms in Eq. (21), are given in previous papers.[1,3,13]

In Eq. (21) the anisotropic angular distribution of the electron scattering has been taken into account by expressing each of the differential scattering cross sections as an expansion in zeroth-order Legendre polynomials. Thus, if

$$I^k(\epsilon,\theta)=\sum_{j=0}^{\infty}\frac{(2j+1)}{4\pi}Q_j^k(\epsilon)P_j(\cos\theta) , \tag{22}$$

then

$$Q_j^k(\epsilon)=2\pi\int_0^\pi I^k(\epsilon,\theta)P_j(\cos\theta)\sin\theta\, d\theta . \tag{23}$$

Here the superscript k indicates the type of collision process, the subscript j indicates the degree of the Legendre polynomial and $I^k(\epsilon,\theta)$ is the differential cross section[13] for electron scattering through an angle θ for process k. Thus, for $Q_0^0(\epsilon)$ the $j=0$ and $k=0$ designate the spherically symmetric component of the elastic scattering cross section, i.e., the "total" elastic cross section. In Eq. (2) we also define a total scattering cross section for all collisions $Q_T(\epsilon)$ by

$$Q_T(\epsilon)=\sum_{k=0}^{p}Q_0^k(\epsilon)+Q_0^i(\epsilon) , \tag{24}$$

an elastic momentum transfer cross section $Q_m(\epsilon)$ by

$$Q_m^0(\epsilon)=Q_0^0(\epsilon)-Q_1^0(\epsilon) , \tag{25}$$

and the ionization cross sections $q_{\rm sec}^i(j,u,\epsilon)$ and $q_{\rm sca}^i(j,u,\epsilon)$ as the Legendre polynomial components of the differential cross sections for the production of secondary and scattered primary electrons of energy ϵ for a primary electron of energy u.

Since we have shown in III that transport and rate coefficients are relatively insensitive to the details of the product electron energy distribution resulting from ionization, we will present in this paper results only for the assumption that each of the product electrons has an energy equal to one half of the available energy. In this case each of the integrals in Eq. (21) is replaced by

$$(2\epsilon+u_i)Q_j^i(2\epsilon+u_i)f_j(2\epsilon+u_i) . \tag{26}$$

In this paper we will compare results obtained for isotropic and anisotropic scattering, while keeping the elastic momentum-transfer cross section constant. The importance of the momentum transfer cross section in the theory of electron transport can be seen by reviewing the equations for the conventional two-term spherical-harmonic expansion solution of the Boltzmann equation, Eqs. (20) and (21) for $m=2$, and (in this paragraph only) treating ionization as an excitation processes. For $j=0$ the collision operator is

$$C[f_0(\epsilon)]=-\sum_{k=1}^{p}[\epsilon Q_0^k f_0(\epsilon)-(\epsilon+\epsilon_k)Q_0^k(\epsilon+\epsilon_k)f_0(\epsilon+\epsilon_k)]+\frac{2m}{M}\frac{d}{d\epsilon}[\epsilon^2 Q_m^0(\epsilon)f_0(\epsilon)] , \tag{27}$$

while for $j=1$ it is

$$C[f_1(\epsilon)] = -\epsilon Q_m^0(\epsilon) f_1(\epsilon) - \sum_{k=1}^{p} \epsilon Q_0^k(\epsilon) f_1(\epsilon) + \sum_{k=1}^{p} (\epsilon+\epsilon_k) Q_1^k(\epsilon+\epsilon_k) f_1(\epsilon+\epsilon_k) . \quad (28)$$

We see that in both of these equations the effects of elastic collisions are represented by the momentum-transfer cross section $Q_m^0(\epsilon)$. In particular, in the usual application of the conventional two-term approximation,[20] where the inelastic cross sections are assumed to be small compared to the elastic cross section, the only cross section entering Eq. (28) is $Q_m^0(\epsilon)$. For this reason we have chosen to make comparisons of the isotropic and anisotropic models of N_2 by keeping the elastic momentum-transfer cross section constant rather than by keeping the total elastic cross section $Q_0^0(\epsilon)$ constant as was done by Kunhardt and Tzeng.[9] On the other hand, since we have shown in III that the term representing the reentry of anisotropic inelastic scattered electrons in Eq. (21) can often be neglected, we will keep the total inelastic cross sections $Q_0^k(\epsilon)$ constant. Note that the inelastic momentum-transfer cross section implied by Eq. (21) and analogous to Eq. (25), is not the same as that needed for use in fluid models of electron motion. See Appendix A.

In summary, we will present results in this paper for two models of electron scattering in N_2. One model uses the full set of anisotropic scattering cross sections and will be referred to as the anisotropic model. In the second model we will use the anisotropic factor $Q_1^0(\epsilon)/Q_0^0(\epsilon)$ to obtain the momentum-transfer cross section for elastic scattering $Q_m^0(\epsilon)$. We will set all $Q_j^k(\epsilon)/Q_0^k(\epsilon)$ for $j \geq 1$ equal to zero. Thus, we use $Q_m^0(\epsilon)$ for the elastic cross section and the various $Q_0^k(\epsilon)$ or total cross sections for inelastic scattering. This model will be referred to as the isotropic inelastic model and is the model used in most previous solutions of the electron Boltzmann equation.[13,20] Note that this model does not assume isotropic elastic scattering as is often stated.

III. CROSS SECTIONS

In this section we present the set of anisotropic collision cross sections for electrons in N_2 which we have assembled and used to investigate the effects of anisotropic scattering on the electron energy distributions and on the transport and reaction-rate coefficients. Because of the importance of collisions at high electron energies, we have examined much more thoroughly than previously the

TABLE I. Ratios of spherical-harmonic components of differential scattering cross sections for N_2.[a]

Process	Q_1^k/Q_0^k	Q_2^k/Q_0^k	Q_3^k/Q_0^k	Q_4^k/Q_0^k	Q_5^k/Q_0^k
Elastic scattering (10^{-2}–10^4)[b]	$-\dfrac{0.2\epsilon^{1/2}}{0.025+\epsilon^{1/2}}$	$-\dfrac{0.04\epsilon}{0.01+\epsilon}$	$\dfrac{0.7\epsilon}{65+\epsilon}$	$\dfrac{0.61\epsilon^2}{2000+\epsilon^2}$	$\dfrac{0.55\epsilon^2}{4000+\epsilon^2}$
	$+\dfrac{1.2[16\epsilon^{1/2}+\epsilon]}{[100+16\epsilon^{1/2}+\epsilon]}$	$+\dfrac{1.04\epsilon(2400+\epsilon)}{[60\,000+3000\epsilon+\epsilon^2]}$	$+\dfrac{0.3\epsilon}{3000+\epsilon}$	$+\dfrac{0.39\epsilon}{5000+\epsilon}$	$+\dfrac{0.45\epsilon}{5000+\epsilon}$
Resonant vibrational excitation (1.7–3.6)	0	$\frac{5}{7}$	0	$\frac{8}{7}$	0
$A^3\Sigma_u^+, B^3\Pi, W^3\Delta$ (7–50)	$-\dfrac{\epsilon^2}{1500+\epsilon^2}$	$\dfrac{\epsilon^2}{10^4+\epsilon^2}$	0[c]	0	0
$C^3\Pi$ (11–50)	−0.2	0	0	0	0
$a^1\Pi_g$ (8.5–500)	$\dfrac{200\,000+160\epsilon^2+\epsilon^4}{200\,000+2600\epsilon^2+\epsilon^4}$	$\dfrac{\epsilon^2}{1600+\epsilon^2}$	$\dfrac{\epsilon^2}{3500+\epsilon^2}$	$\dfrac{\epsilon^2}{3500+\epsilon^2}$	$\dfrac{\epsilon^2}{3500+\epsilon^2}$
"Sum of singlets" (13–500)	$\dfrac{\epsilon^2}{2500+\epsilon^2}$	$\dfrac{\epsilon^2}{2500+\epsilon^2}$	$\dfrac{\epsilon^2}{3500+\epsilon^2}$	$\dfrac{\epsilon^2}{3500+\epsilon^2}$	$\dfrac{\epsilon^2}{3500+\epsilon^2}$

[a]Note that from Fig. 3 we would now choose somewhat lower values for D in some cases, e.g., 1000 and 300 for $A^3\Sigma_u^+$, $B^3\Pi$, and $w^3\Delta$ and for $j=1$ and 2, respectively.

[b]The numbers in parentheses give the energy range in eV of the data used to obtain the formulas in this table. Only in the cases of the singlet states are the formulas of significance outside these energy ranges.

[c]From Fig. 3 we would now take this entry to be $-\epsilon^2(5000+\epsilon^2)^{-1}$.

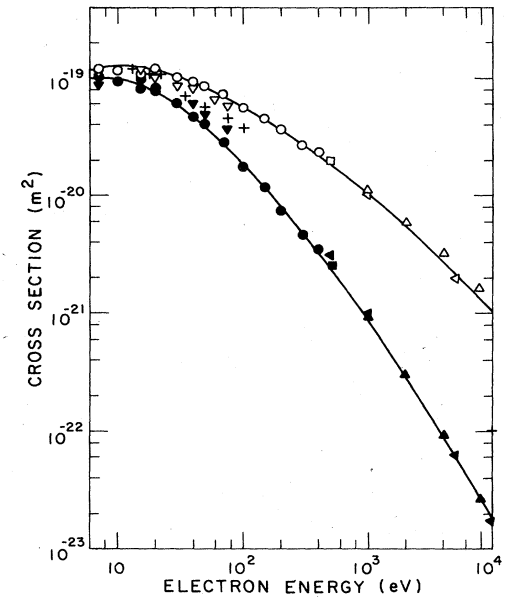

FIG. 1. Elastic scattering cross sections for N_2 The upper curve and the open points and crosses are the total cross sections, while the lower curve and the solid points are the momentum-transfer cross sections. Symbols and authors are the following: □, ■, Bromberg (Ref. 23); +, Finn and Doering (Ref. 23); ▽, ▼, Srivastava *et al.* (Ref. 23); ○, ●, Shyn and Carignan (Ref. 23); △, ▲, Riley *et al.* (Ref. 24); ◁, ◀, Strickland *et al.* (Ref. 24).

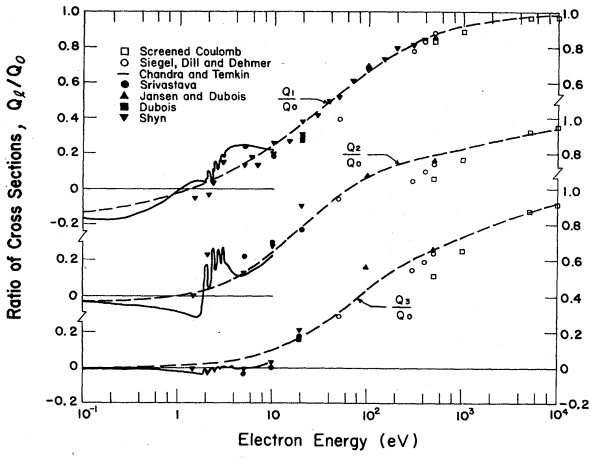

FIG. 2. Ratios of spherical-harmonic components calculated from elastic differential scattering cross-section data. Here we have suppressed the superscript 0 on the Q_j^0 symbols. The dashed curves are our empirical fits listed in Table I. The solid points are from experiment, while the open points and solid curve are from theory. Symbols and authors are the following: ■, DuBois *et al.* (Ref. 28); ▲, Jansen *et al.* (Ref. 23); ●, Srivastava (Ref. 23); ▼, Shyn and Carignan (Ref. 23); □, Riley *et al.* (Ref. 24); ——, Chandra and Temkin (Ref. 29); ○, Siegel *et al.* (Ref. 29).

high-energy cross-section data available in the literature. In particular, we have considered experimental and theoretical determinations of angular distributions of elastically and inelastically scattered electrons and have developed analytical fits to these data which are useful for numerical calculations using the spherical-harmonic expansion technique.[1,2] For these purposes, the most convenient method of discussing and tabulating the differential scattering data is to analyze the expermental data in terms of the spherical-harmonic components of the differential cross section $Q_j^k(\epsilon)$ as defined in Eqs. (21)—(23). The results are summarized in Table I. Rather than present the energy dependences of the total cross sections for the 23 inelastic collision processes used in this paper we have made them available in report form.[21]

In general our approach in deriving this set of cross sections for $\epsilon > 7$ eV has been to use experimental electron beam data and theory, except when such a procedure leads to discrepancies with swarm data or when there are ambiguities in the beam data. For electron energies below 7 eV we have used the results of swarm analyses except for the energy dependences and relative magnitudes of the cross sections for vibrational excitation in the energy range from 1.7 to 3.6 eV. We discuss first the elastic scattering data and then the inelastic scattering data.

A. Elastic scattering

The effective momentum-transfer cross sections $Q_m^e(\epsilon)$ of Engelhardt, Phelps, and Risk,[22] to be referred to as EPR, were retained at electron energies below 7 eV. The elastic momentum-transfer cross section $Q_m^0(\epsilon)$ was obtained from $Q_m^e(\epsilon)$ by subtracting the sum of the vibrational excitation cross sections $\sum Q_0^v(\epsilon)$ which are to be discussed later. The resultant curve should then be smoothed to take into account differences in the effective energy resolution of the swarm analysis and the beam experiments. In the case of the calculations which we have designated in Sec. II as isotropic inelastic scattering calculations, the total elastic cross section is set equal to the elastic momentum-transfer cross section of EPR, i.e., $Q_0^0(\epsilon) = Q_m^0(\epsilon)$. In calculations where anisotropic scattering was considered the total elastic scattering cross section $Q_0^0(\epsilon)$ was obtained by multiplying the elastic momentum-transfer cross section from EPR by $Q_0^0/Q_m^0 = (1 - Q_1^0/Q_0^0)^{-1}$, where formulas for Q_1^0/Q_0^0 as a function of electron energy are given in Table I.

At electron energies above 7 eV the total and momentum-transfer elastic cross section were obtained from measurements of total and differential scattering cross sections[23] and from theory.[24] The points of Fig. 1 show the experimental and theoretical data for electron energies between 6 and 10^4 eV, while the smooth curves show the values recommended by Hayashi.[25] The open and closed points are the total and momentum-transfer cross sections, respectively. Note that Hayashi's recommendations are in good agreement with the values used in several analyses[26,27] of swarm data.

In order to limit the amount of tabulated data required and reduce the computation time for calculations which take into account anisotropic scattering we have used tabulated values of the momentum-transfer cross section[21] and simple analytic approximations to the ratios of the

higher-degree spherical-harmonic components of the cross sections Q_j^0 to the total elastic cross section Q_0^0. In terms of these ratios and the tabulated values of Q_m^0, the magnitude of the jth component of the elastic scattering cross section is given by

$$Q_j^0 = Q_m^0 \frac{Q_j^0}{Q_0^0}\left[1-\frac{Q_1^0}{Q_0^0}\right]^{-1}. \tag{29}$$

Here we have suppressed the dependence on electron energy ϵ. The use of simple analytical approximations to the Q_j^k/Q_0^k values averages through the structure present, for example, near 2 eV and is justified by the relatively slowly varying electron energy distributions.

Figure 2 shows values of the ratios Q_1^0/Q_0^0, Q_2^0/Q_0^0, and Q_3^0/Q_0^0 determined from experiment[23,28] and theory.[24,29] In a few cases the theoretical results are available in a form equivalent to Q_j^0, but in most cases it was necessary to resolve plotted differential scattering cross-section data into spherical-harmonic components with the associated uncertainties resulting from incomplete data at small and large scattering angles. The dashed curves of Fig. 2 show the values of the analytical expressions given in Table I and used to approximate the experimental and theoretical data. In view of the structure in the theoretical curves near 2 eV and the scatter in the higher-energy data shown in Fig. 2, it does not seem worthwhile to attempt better fits to the data at this time. As listed in Table I, we carried out the analysis to $j=5$ in anticipation of six-term solutions of the Boltzmann equation. Of some concern to us is the tendency of the Q_j^0/Q_0^0 ratios to saturate at values well below unity at high-electron energies. This behavior may indicate a tendency of experiments and/or our analyses to inaccurately represent the forward scattering peak of the differential scattering cross section. Accordingly, we used a smooth interpolation between ratios determined from experimental data at energies below 300 eV and ratios determined from theory at energies above 5 keV.

B. Rotational and vibrational excitation

Electron-beam experiment[30] and theory[29,31] have shown that rotational excitation cross sections are very large in the vicinity of 2 eV. Because of the shortage of cross-section data and in order to reduce the computer space required to store and use the very large number of energy-dependent rotational excitation cross sections in the resonance region, we have used the single-level approximation for the cross section for rotational excitation as derived from gas-heating data. See Appendix B. This cross section has a magnitude equal to the sum of the magnitudes of the vibrational excitation cross sections discussed next and is assigned an energy loss of 0.02 eV. Using this cross section we find that for the E/n considered in this paper the energy loss to resonance rotational excitation is as much as 11% of the input energy at mean electron energies near 0.6 eV. The rotational excitation was assumed to be isotropic, although now one could use the formulas of Wong and Dubé[30] for the resonance region.

The cross sections for electron excitation from the $v''=0$ vibrational level of $X^1\Sigma_g^+$ of N_2 to higher vibrational levels ($v'=1$ to 8) of the $X^1\Sigma$ state come from a variety of sources. The cross section for excitation of the $v'=1$ level at electron energies below 1.7 eV is that found by EPR (Ref. 22) with a small modification near 1.5 eV to allow for resonance rotational excitation. For resonance excitation of the $v'=1$ to 8 levels at electron energies between 1.7 and 3.6 eV, we have used as a reference set the results of Schulz[32] as normalized to Spence, Mauer, and Schulz[33] by Kieffer.[4] Note that these resonance cross sections show larger magnitudes for the higher vibrational levels relative to the cross section for excitation of the $v'=1$ level than do the earlier results of Schulz[35] which we have used in previous analyses[1-3,22] of N_2. The magnitude of the resonance vibrational excitation cross sections was made adjustable through the use of a scale factor multiplying the input or reference set. Except as noted, the multiterm calculations reported in this paper used a scale factor of 1.5 for the resonance portion of the vibrational cross section since this gives a better fit to electron-transport data than the value of 1.9 appropriate to the earlier two-term calculations.[17] The cross section for excitation of the $v'=1$ level at energies above 3.7 eV is based on the experimental results of Pavlič *et al.* and Truhlar *et al.*[36] The excitation of vibrational levels with $v'>1$ was neglected for energies above 3.6 eV. For calculations in which vibrational excitation resulting in anisotropic scattering was considered, we used the approximate angular distribution given by Polak and Slovetskii.[37] See Table I. Since this formula gives $Q_1^v=0$ for all v', the use of $Q_m^e=Q_m^0+\sum Q_0^v$ in the $j=1$ equation for the electron energy distribution, as discussed in III, is exact in the region of the 2-eV resonance.

C. Electronic excitation

Since the $N_2(A^3\Sigma_u^+)$ state is the lowest energy electronic state we have made an approximate allowance for the spread in energies of the various vibrational levels, i.e., the cross sections have been separated into three groups representing transitions from $v''=0$ of the X state to levels with $v'=0$–4, $v'=5$–9, and $v'>10$ of the A state. For incident electron energies above 11 eV we have used a common energy dependence and total magnitude based on Cartwright *et al.*[38] (CTCW) and have weighted the partial cross sections using Franck-Condon factors determined from optical spectra.[39] The energy dependences of the cross sections at energies below 11 eV are such that the total N_2 triplet cross section is consistent with the energy dependence[40] of Olmsted, Newton, and Street and of Borst.

The cross section used for the $C^3\Pi_u$ state at energies between 15 and 50 eV is from CTCW, while at energies below 15 eV the cross section is based on an average of recent measurements.[41] The area under the resonant peak portion of the $E^3\Sigma_g^+$ cross section is from Borst, Wells, and Zipf,[42] while the location in energy is from more recent experiments.[41] The $E^3\Sigma_g^+$ cross section for energies between 15 and 50 eV is from CTCW. The cross sections for excitation of the $B^3\Pi$, $W^3\Delta$, $B'^3\Sigma_u^-$, $a'^1\Sigma_u^-$, $a^1\Pi_g$, $w^1\Delta_u$, and $a''^1\Sigma_g^+$ states for energies below 50 eV are based on CTCW. The triplet cross sections just described

are based on electron beam data. Agreement between calculated and measured $C^3\Pi_u$ excitation coefficients[18] and ionization coefficients[7] at $E/n < 300$ Td, was found[18] by adjusting the magnitudes of these cross sections. We use factors of 2.0 for the $C^3\Pi_u$ state and 0.67 for all other triplet states.

The choice of cross sections for excitation of the important states at the higher-electron energies is based on the analyses of Zipf and McLaughlin[43] and of Jackman *et al.*[44] In particular, the Zipf and McLaughlin results have been used to construct the sum of cross sections for the excitations of the various $^1\Pi_u$ states, the $c'^1\Sigma_u^+$ and $b'^1\Sigma_u^+$ states, and unidentified states with energy losses of 15.8 and 17.3 eV. This combined cross section will be identified as the "sum of singlets." Note that at energies above about 50 eV it is much larger than the sum of the corresponding singlet cross sections obtained by Chutjian *et al.*[45] The cross sections for excitation of the $a^1\Pi_g$ and $a''^1\Sigma_g^+$ state of CTCW were extended to higher energies using the energy dependences of Jackman *et al.*[44]

The ionization cross section used is based on Rapp and Englander-Golden and Schram *et al.*,[46] while the secondary energy distribution is a delta function with half of the available energy as indicated by Eq. (26). A better approximation would have been a delta function with the correct mean secondary electron energy.[3,47]

The ratios of the spherical-harmonic components of the differential scattering cross sections for electronic excitation at energies from 10 to 50 eV are based on the data of Cartwright *et al.*[48] and of Chutjian *et al.*[45] Representative spherical-harmonic components of the cross sections for the $A^3\Sigma_u^+$ and $b^1\Pi_u$ states are shown in Fig. 3. The differential scattering data of Lassettre and co-workers[49] has been used to obtain the cross-sections ratios shown in Fig. 3 for the $b^1\Pi_u$ state at 500 eV. We have used the results for the $b^1\Pi_u$ state as representative of the group of allowed singlet excitation cross sections. Of particular importance in our calculations is the pronounced forward scattering[50] for the sum of singlet states. Our fits to these and similar plots for other states are listed in Table I. It should be kept in mind that these formulas may be meaningful only over the energy range for which the cross sections are large enough to allow measurement of $I^k(\epsilon,\theta)$, i.e., the energy ranges shown in parentheses in Table I. We have not attempted to convert the predicted phase shifts of theory[51] into spherical-harmonic components of the excitation cross sections. A notable feature of the lower triplet states is the tendency for backward scattering, i.e., the Q_1^k/Q_0^k values are negative. Also note that we would have obtained somewhat better fits to experiment in Fig. 3 if we had written the empirical formulas in terms of $(\epsilon-\epsilon_k)$ instead of ϵ, i.e., for many of the excited states of N_2 the experimental electron scattering approaches isotropy at threshold.

The amount of detail required to satisfactorily represent the experimental angular distributions[47] for the two electrons produced in electron-impact ionization is not clear. Approximate angular distributions have been given[52] by Jackman and Green and by Wilhelm and Winkler. We have adopted a similar approximation in which the low energy or secondary electron[3] is assumed to be produced with an isotropic angular distribution, while the high energy or scattered primary electron is given the same angular distribution as for the sum of the singlet states.

A test for consistency among our set of cross sections is given in Fig. 4 where the curves show values of the total cross section $Q_T(\epsilon)$, the total elastic cross section Q_0^0, the

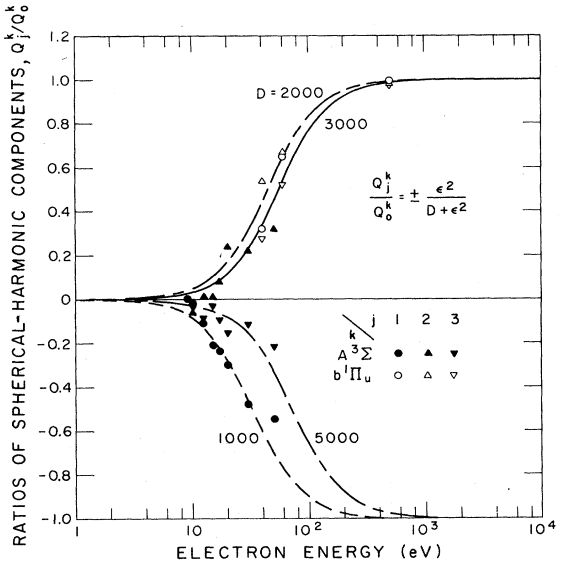

FIG. 3. Spherical-harmonic components of differential cross sections for electron excitation of $A^3\Sigma_u^+$ and $b^1\Pi_u$ states. The points of $\epsilon < 100$ eV are calculated from the experimental data of Ref. 38 for the values of j indicated in the inset. The points for 500 eV are from Ref. 49. The smooth curves are calculated for various values of D. The formulas adopted are listed in Table I.

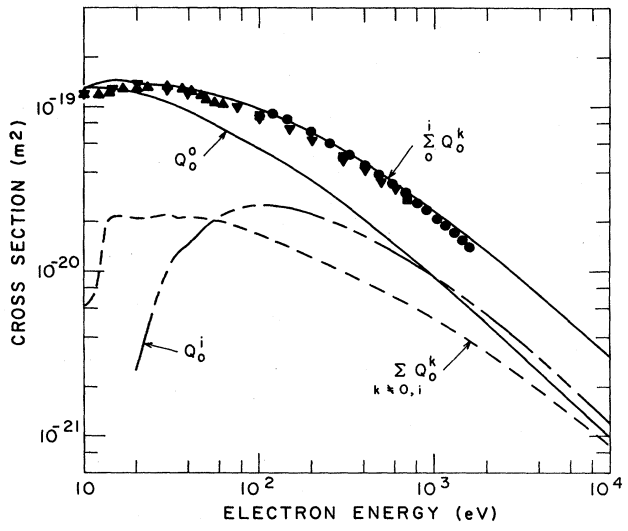

FIG. 4. Total electron scattering cross sections for N_2. The uppermost curve is our sum of all total cross sections Q_0^k. Our total elastic, total ionization, and sum of the total inelastic cross sections are labeled Q_0^0, Q_0^i, and $\sum Q_0^k$ for $k\neq 0,i$, respectively. Symbols and authors are the following: ■, Blaauw *et al.* (Ref. 53); △, Kennerly (Ref. 53); ● Dalba *et al.* (Ref. 53); ▼, Hoffman *et al.* (Ref. 53).

sum of the excitation cross sections Q_0^k for all k not equal to 0 or i, and the total ionization cross section Q_0^i. The solid points show experimental values of the total cross section.[53] Note that the elastic, excitation, and ionization cross sections become comparable at the higher-electron energies and that the sum of these cross sections, as shown by the upper solid line, is equal to the total cross section to within the combined uncertainties. At electron energies above about 50 eV these curves agree reasonably well with the model of Jackman and Green.[52] It is not clear which of the cross sections should be reduced in order to improve the agreement with the total cross-section measurements. The excitaton cross sections would seem to be the most subject to error, although there is some disagreement among the measured ionization cross sections.[46]

The principal improvements in the magnitudes and energy dependences of cross sections discussed in this paper from those of our previous work[17,18,22] are (a) the significantly larger electronic excitation cross sections at high energies, (b) more accurate representations of electron-beam data for excitation of the $C^3\Pi_u$ and $E^3\Sigma_g^+$ states while retaining consistency with excitation coefficient data, and (c) the introduction of an effective resonance rotational excitation cross section. We have not attempted to optimize the cross sections by comparison with transport and excitation coefficient data, although we will show in Sec. V that the agreement of calculated and experimental swarm data is generally good.

IV. CALCULATED TRANSPORT COEFFICIENTS AND DISTRIBUTION FUNCTIONS

A. Effects of anisotropic scattering

The transport and reaction-rate coefficients calculated using the procedures of Sec. II and the cross sections of Sec. III were used to obtain the data of this section. As an example of these results, the calculated spherically symmetric components of the electron energy distributions $f_0(\epsilon)$ for $E/n=1500$ Td are shown in Fig. 5. Starting from the uppermost curve at high energies the curves show the calculations for six-term anisotropic, six-term isotropic, two-term anisotropic, and two-term isotropic models. We see that at high energies, $\epsilon > 80$ eV, the anisotropic models yield about 20% more high-energy electrons than do the isotropic models. However, at these high energies the largest change is the result of including more terms in the spherical-harmonic expansion, as will be discussed in Sec. IV B. Note that for the two-term approximation the fact that the elastic momentum-transfer cross section was kept constant means that the changes observed in the distribution functions as the result of the change from isotropic to anisotropic scattering are due to the effects of the dipole ($j=1$) components of the inelastic scattering. The somewhat larger change in $f_0(\epsilon)$ observed when changing the scattering model with the six-term approximation includes the effects of higher-degree components of the elastic and inelastic scattering. Although not readily seen in Fig. 5, the curves of $f_0(\epsilon)$ for the anisotropic and isotropic models cross such that at energies

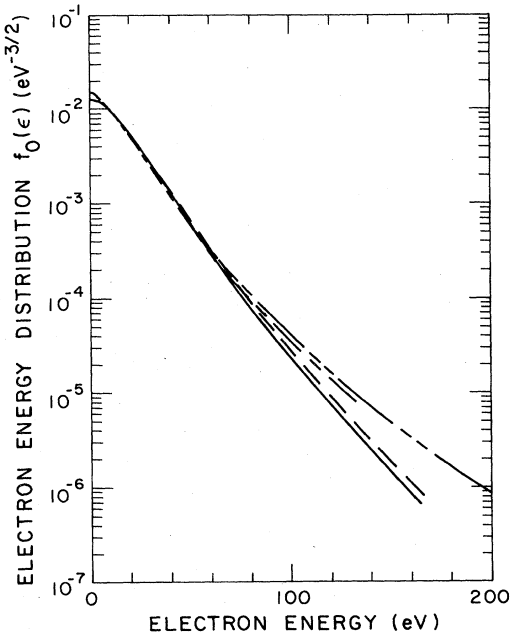

FIG. 5. Spherically symmetric component of electron energy distribution functions showing effects of anisotropic scattering and multiterm spherical-harmonic approximations. $E/n=1500$ Td. Symbols and assumptions are the following: ——, isotropic and two-term; — — —, anisotropic and two term; —·—·—, isotropic and six term; --—--, anisotropic and six term.

below the mean energy (23 eV) the isotropic model has about 5% more electrons. Presumably the high-energy effect results from the reduced large-angle scattering for the anisotropic model. The change in $f_0(\epsilon)$ at low energies reflects, in part, the renormalization of the distribution to account for the change in the number of high-energy electrons. The electron energy distributions, such as shown in Fig. 5, are used to calculate the transport, excitation, and ionization coefficients. Except where stated otherwise, we estimate the accuracy of the calculated coefficients to be $\pm 1\%$. However, calculated changes in the coefficients with cross-section sets should be more accurate, e.g., $\pm 0.5\%$. These estimates are based on tests of the sensitivity of the calculations to the choice of energy grid, etc. Note that for $E/n=20$ Td, but not for 10 or 40 Td, the changes in coefficients with energy grid were comparable with the small changes in coefficients produced by changes in the scattering model or the number of spherical harmonics.

The calculations of changes in transport and rate coefficients made using the six-term approximation for the anisotropic and isotropic models are summarized in Fig. 6. The curves of Fig. 6 show the values of the fractional change in the transport or reaction coefficient when the scattering is changed from the isotropic model to the anisotropic model, e.g., $\hat{W}=(W_{\rm iso}-W_{\rm aniso})/W_{\rm aniso}$. We see that for E/n below 500 Td or mean energies below 9 eV the errors in the coefficients resulting from the isotropic scattering assumption are less than about 2% as found in previous analysis of model atoms and molecules.[4,5] Of course even these errors are important for the analyses of precision transport data.[13] For E/n above 500 Td the

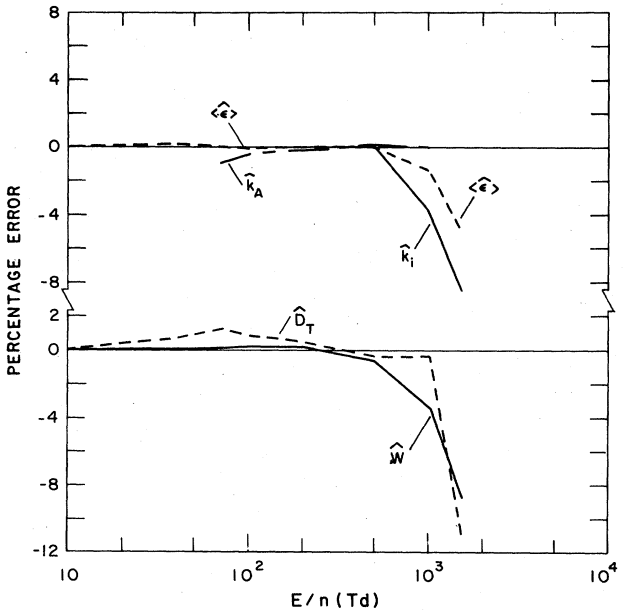

FIG. 6. Percentage change in transport and reaction coefficients caused by change from isotropic to anisotropic scattering models. Coefficients and symbols are the following: $\hat{\epsilon}$, average energy; $\hat{k}_A$, triplet excitation; $\hat{k}_i$, ionization; $\hat{D}_T$, transverse diffusion; $\hat{W}$, drift velocity. The lines simply connect calculated values.

curves of Fig. 6 show that most of the errors increase rapidly with E/n. The large difference in the errors for the triplet excitation coefficient and the ionization coefficient at high E/n occurs because of the crossover of the electron energy distributions with and without anisotropic scattering shown in Fig. 5 and because the triplet excitation cross-sections peak at energies near the crossover while the ionization cross section peaks at energies above the crossover. The higher mean electron energy found with anisotropic scattering is consistent with the larger number of high-energy electrons shown in Fig. 5, while the higher-electron drift velocity is consistent with a lower contribution of inelastic scattering to the momentum-transfer cross section in this case. The much larger transverse diffusion coefficient D_T for the anisotropic model at 1500 Td is at first surprising in view of the decrease in D_T/ν found by Kücükarpaci and Lucas[9] for N_2 and by Haddad *et al.*[5] for H_2. However, it is accompanied by a much larger increase in D_L so that the relative increases are as expected. We have not shown the errors for the longitudinal diffusion coefficient since questions have been raised[54] regarding the accuracy of the multiterm calculations of D_L for N_2 and because of erratic results obtained in the present calculations. Unfortunately, the issue is clouded by the question of runaway effects, i.e., Kunhardt and Tzeng[9] find that their set of anisotropic cross sections results in the failure of the calculated diffusion coefficients to reach steady-state at $E/n=1500$ Td as required for the validity of the hydrodynamic model. At lower E/n their results show changes with the scattering model which are similar to ours in sign but usually larger in magnitude. An important question here is the precision of their Monte Carlo calculations. The changes in W and $\langle\epsilon\rangle$ shown in Fig. 6 are significantly smaller than those calculated by Kücükaparci and Lucas[9] using less accurate differential scattering data.

B. Effects of two-term approximation

In the course of the present calculations we have extended the comparisons of results obtained using the two-term and six-term spherical-harmonic expansions to higher E/n for electrons in N_2. Representative results for the electron energy distributions at high E/n (1500 Td) are shown in Fig. 5, where at high energies the lower pair of curves were calculated using the two-term approximation and the upper pair were calculated using the six-term approximation. The relatively large change in the numbers of high-energy electrons is ascribed to the failure of the two-term spherical-harmonic approximation when the ratio of the inelastic cross section to the elastic cross section is large. This tendency toward streaming in the direction of the acceleration is in part due to decreasing inelastic cross sections with increasing electron energy at high energies. We have verified the relation between large fractional excitation cross sections and the error in $f_0(\epsilon)$ for the two-term approximation using model cross sections and a simplified Boltzmann equation.[6] Note that for the high E/n of Fig. 5 the energy gained per elastic collision by low-energy electrons is about 10 eV.

The results of the calculations of the errors in transport and rate coefficients for the two-term approximation relative to the six-term approximation are summarized in Fig. 7. These calculations are for the anisotropic model. At low and moderate E/n these results are similar to those of I for isotropic scattering. Particularly noticeable are the increasing errors in the triplet excitation coefficients and the ionization coefficients as E/n decreases. These errors are caused by the systematic deficiency in high-energy electrons for the two-term approximation in the presence of large inelastic cross sections.[2,6] At high E/n the increase in the error in the calculated transverse dif-

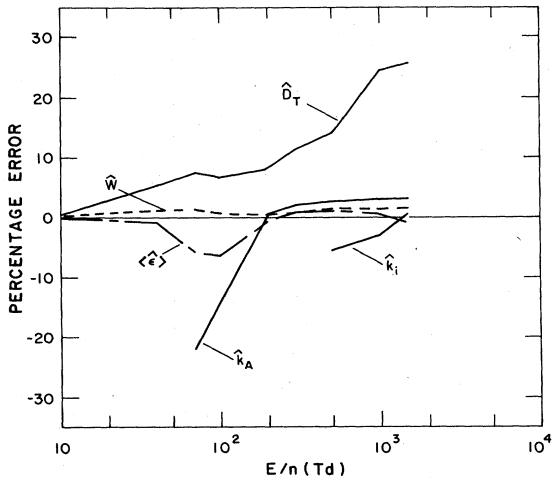

FIG. 7. Percentage change in transport coefficients caused by change from two-term to six-term spherical-harmonic solution of Boltzmann equation. The symbols are the same as for Fig. 6.

fusion coefficient with E/n shown in Fig. 7 is particularly large and is presumably associated with the inability of the two-term approximation to describe properly the tendency of the distribution function to constrict radially. The tendency of the error in the ionization coefficient to become positive at high E/n may be because the correct electron energy distribution tends to have a much larger number of very-high-energy electrons where the ionization cross section is decreasing. This incipient runaway effect needs to be considered further.

V. COMPARISON WITH EXPERIMENT

The objectives of this section are (a) to compare our calculations of transport coefficients with the available experimental data and (b) to draw attention to and make comparisons among theory and experiment for the two types of ionization and excitation coefficients, i.e., the temporal and spatial coefficients, discussed in Sec. II. For the latter purposes, it is particularly important to properly classify the various ionization and excitation experiments at very high E/n before attempting comparisons with theory, rather than to use relationships valid at lower E/n to convert from one coefficient to the other as is commonly done. We will see that there remain significant discrepancies between theory and experiment at very high E/n. It appears that both theory and experiment need improvement.

Figures 8—10 show comparisons of calculated and experimental transport, excitation, and ionization coefficients for electrons in N_2 at moderate and high E/n. The solid curves show the results of the calculations made using the anisotropic cross section set discussed in Sec. III and the six-term spherical-harmonic expansion, while the dashed curves show the results of calculations made using the isotropic inelastic model and the two-term spherical-harmonic expansion form discussed in Sec. III. The points are from experimental data selected as the most accurate and/or recently available data in the various E/n ranges.

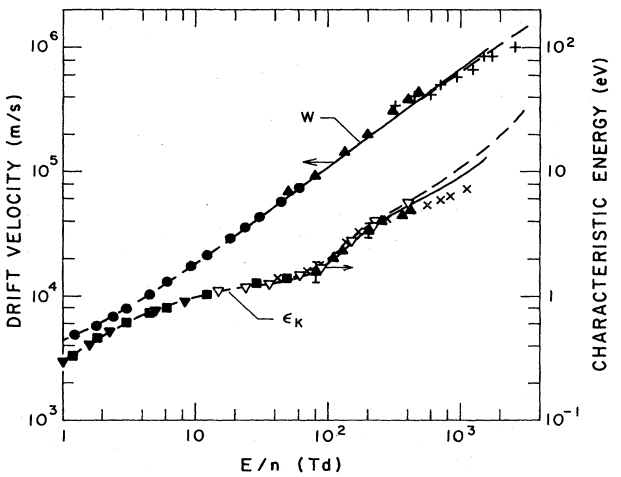

FIG. 8. Electron drift velocity W and characteristic energy ϵ_K versus E/n for N_2. The anisotropic cross section set from Sec. III and the six-term solution of the Boltzmann equation were used to calculate the solid curves. The isotropic inelastic set and the two-term approximation were used to obtain the dashed curves. The points show selected experimental data. Symbols and authors are the following: ● Lowke (Ref. 55); △, Fletcher and Reid (Ref. 55); ▼, Warren and Parker (Ref. 56); ■, Crompton and Sutton (Ref. 56); +, Schlumbohm (Ref. 55); ×, Kontoleon *et al.* (Ref. 56); ▽, Roznerski and Leja (Ref. 56).

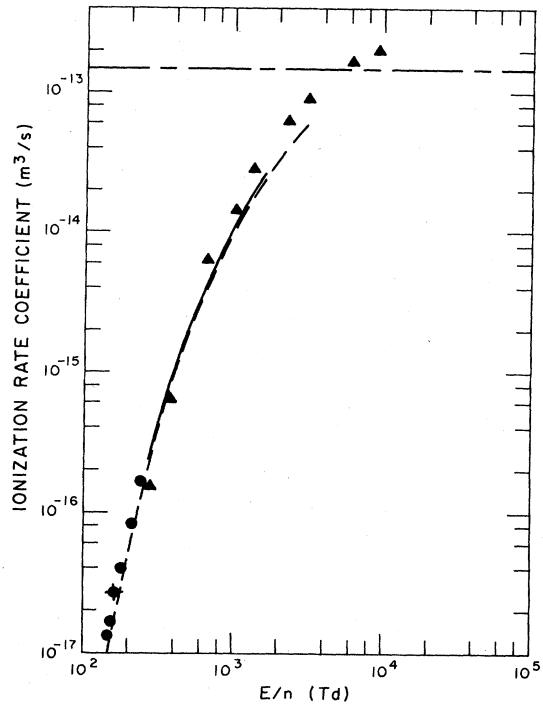

FIG. 9. Comparison of theoretical and experimental temporal growth constants ν/n for the electron density in N_2 at high E/n. The calculated curves are designated as in Fig. 8. The points show experimental data with the following symbols and authors: ●, Frommhold (Ref. 57); +, Dibbern (Ref. 57); ▲, Felsenthal and Proud (Ref. 57).

For E/n below 100 Td there is generally good agreement between our calculations and experimental[55] time-of-flight drift velocities shown in Fig. 8. It must be kept in mind that our drift velocities are calculated without the ionization corrections given by the second term in Eq. (5) and the resultant iteration implied by Eq. (10). From the calculations of Taniguchi *et al.*[26] we expect that our calculated drift velocities will be lower than the experimental time-of-flight velocities when ionization effects are important. Thus at E/n near 400 Td in Fig. 8, the two-term results of Taniguchi *et al.* and our approximate calculations show that the second term of Eq. (5) increases the drift velocity by about 10% and so improves agreement with experiment. However, the lower experimental values observed at higher E/n are not predicted[26] by the theory of Sec. II and may be the result of inapplicability of the hydrodynamic model or of the difficulties of measurement of such high drift velocities. Because of the common application of the two-term, isotropic inelastic model, we show the results of this model by the dashed curve. As is also indicated by Figs. 5 and 6 this model is

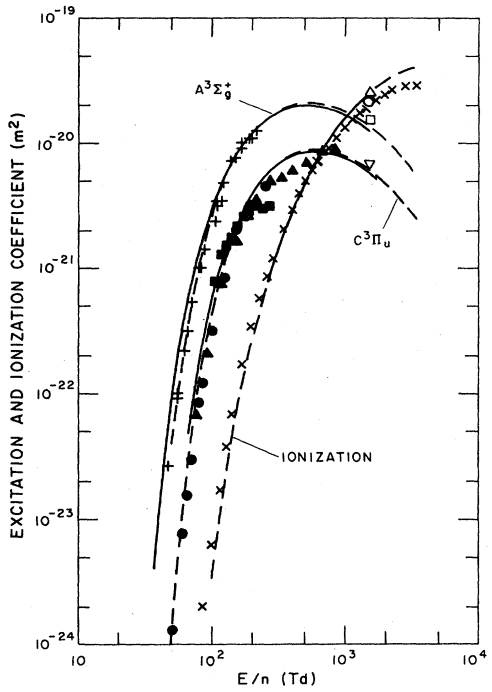

FIG. 10. Comparison of theoretical and experimental spatial excitation and ionization coefficients for electrons in N_2. The curves are calculated as in Fig. 8. The symbols and authors for the selected experimental data are the following: +, Levron and Phelps (Ref. 17); △, Legler (Ref. 18); ●, Tachibana and Phelps (Ref. 18); ■, Urešović *et al.* (Ref. 18); ×, Haydon and Williams (Ref. 59). The open points are calculated using the exponential spatial growth assumption as discussed in the text.

satisfactory for many purposes for $E/n < 500$ Td.

Experimental values of the characteristic energy, $\epsilon_K = eD_T/\mu$, are usually determined by fitting steady-state solutions of the hydrodynamic equation Eq. (3) to measurements of current ratios in a drift tube with a restricted area cathode.[13] The comparison in Fig. 8 of calculated values of characteristic energy shows reasonable agreement with experiment[56] at E/n below 40 Td. For E/n between 40 and 200 Td the comparison is made difficult by the differences among experiments and the large uncertainties assigned to some of the data. This is unfortunate since it is this E/n range which is important in comparisons of measured excitation and ionization coefficients, such as shown in Figs. 9 and 10. Also noticeable are the differences in the ϵ_K values calculated using the isotropic cross-section set and the two-term expansion versus the anisotropic set with the six-term spherical-harmonic expansion. As shown in Sec. IV most of the differences arise from the use of the different spherical-harmonic approximations. The decrease in the measured ϵ_K values below our calculated values at E/n above 300 Td may be caused by our failure to include ionization effects in the calculations for the mobility and transverse diffusion coefficient or may be caused by departures from the hydrodynamic limit. The values of ϵ_K for high E/n calculated by Taniguchi *et al.*[26] using the two-term approximation including the ionization correction of Eq. (7) lie between the curves of Fig. 8.

The temporal growth constant ν found by the solution of the Eq. (9) describes the growth of electron density when the effects of electron-density gradients are negligible as when observing the spatially integrated growth of light output or of electron current in a pulsed Townsend experiment[11,16,57] or the growth of ionization in magnetically confined discharge with a toroidal electric field.[58] In Fig. 9 we compare measured and calculated temporal growth constants. At the lower E/n the experimental values lie somewhat above the two-term, isotropic calculations as expected from the systematic errors in the two-term calculations.[6] At high E/n the fact that the experimental results are too high may be the result of difficulties of interpretation of the measurements.[57] Runaway effects, if present, would be expected to reduce the temporal growth constant below the maximum value of the ionization rate coefficient for monoenergetic electrons indicated by the chain line.

Since most measurements of excitation and ionization coefficients are made using the steady-state drift-tube technique, Fig. 10 shows calculated and measured spatial growth coefficients as a function of E/n. The normalized spatial ionization coefficients α_i/n shown by the smooth curves of Fig. 10 were calculated from the values of ν and W neglecting the $\alpha_i^2 D_L$ term in Eq. (13). The α_i/n values calculated using Eq. (13) are higher by as much as a factor of 1.6 at $E/n = 1500$ Td. In order to test these simplified calculations of the spatial growth constant α_i/n, we have solved Eqs. (17)—(21) with $\nu/n = 0$, $m = 2$, and isotropic scattering for $E/n = 1500$ Td. This result is indicated by the open circle in Fig. 10 and is to be compared with the result obtained with $\alpha_i = \nu/W$ as indicated by the open triangle. The ratio of 1.2 is indicative of the expected difference between the solid curve of Fig. 10 and the exact calculation. These comparisons show that there is a cancellation of the effects of the increase in α_i/n caused by the $(\alpha_i/n)^2(nD_L)$ and higher terms in Eq. (13) and the decrease in α_i/n caused by the increase in W resulting from the contribution of ionization in Eq. (5). The agreement between calculated and measured[59] ionization coefficients for E/n less than 1000 Td is good since, as in our previous analysis,[18] most of the electronic excitation cross sections were adjusted, i.e., reduced by a factor of $\frac{2}{3}$ from electron-beam results, in order to obtain the fit. The agreement at higher E/n is also good when one takes into account the correction indicated by the open points. Similar agreement has been found by Taniguchi *et al.*[26]

Figure 10 also compares calculated and measured spatial excitation coefficients for the $A^3\Sigma_u^+$ and $C^3\Pi_u$ states. The measured excitation coefficients for the $A^3\Sigma_u^+$ state[17] are shown as points and are assumed to include the contributions of cascading from all of the triplet states of N_2. The smooth curves were obtained using the conventional procedure of dividing the excitation rate coefficient calculated using $f_0(\epsilon)$, i.e., $k_k = \int Q_0^k(\epsilon) f_0(\epsilon) d^3\epsilon$, by our uncorrected value of W. We note that there is good agreement between the $A^3\Sigma_u^+$ excitation coefficients calculated

using the two-term isotropic model (dashed curve) and experiment, but that at low E/n the values calculated using the anisotropic six-term model (solid curve) model are too high. As shown in Sec. IV the difference is largely due to errors introduced by the two-term model rather than to errors from the isotropic scattering assumption. The better fit for the two-term model is the result of the adjustment of the magnitude of the vibrational excitation cross sections so as to fit the excitation coefficient data rather than to fit transport data. These trade-offs have been examined previously[17] using the two-term approximation. We note that because of the higher excitation coefficients obtained with the six-term approximation, the scaling factor which multiplies the reference set of resonance vibrational cross sections could be raised from 1.5 to 1.9 so that the calculated $A^3\Sigma_u^+$ excitation coefficients fit the experimental values. Evidence for such large vibrational excitation cross sections has been obtained by Schulz[60] using electron-beam techniques. However, this change results in ϵ_K values which are about 3% below the values shown in Fig. 8. This seems outside the spread of the experimental results and the discrepancy found earlier[17] is unresolved. (See *Note added in proof.*) The effect of the spatial gradient on the calculated spatial excitation coefficient at 1500 Td, as calculated using Eq. (16) with Q_0^i replaced by the sum of the triplet Q_0^k values, is indicated by the difference between the dashed curve and the open square. At this E/n the excitation rate coefficient k_{kss} is relatively insensitive to changes in the electron-density distribution caused by the density gradient[26] since the mean electron energy is about equal to the energy of the cross-section maximum. Therefore, the higher α_A/n value is caused principally by the lower value of the V_d used in the analog to Eq. (16) compared to the value of W used to calculate the smooth curves.

Figure 10 shows curves of the spatial excitation coefficients for the $C^3\Pi_u$ state as calculated using the same procedure as for the $A^3\Sigma$ state. Here we include the small contribution of cascading from the $E^3\Sigma_g^+$ state. The experimental data from several experiments are shown by the points. Although the calculated curves for $C^3\Pi_u$ excitation agrees in shape with the results[18] of Tachibana and Phelps and the lower E/n data of Legler, it is higher by 1.3 to 1.9 for low E/n, depending on the technique for solving the Boltzmann equation. This difference between calculation and experiment could be removed by lowering the cross sections for $C^3\Pi_u$ and $E^3\Sigma_g^+$ excitation. On the other hand, the lower E/n data of Urošević *et al.*[18] lies above the calculation at the lower E/n and below it at the higher E/n. The effect of the spatial gradient on the calculated excitation coefficient at 1500 Td is indicated by the difference between the dashed curve and the inverted open triangle. Judging from this calculation and from the calculated corrections to the excitation coefficients for spatial gradient and ionization effects of Taniguchi *et al.*,[26] we cannot explain the deviations from the E/n dependence of our calculations observed in the data of Legler and of Urošević *et al.* at high E/n. Note that the excitation coefficients calculated[26] for the $C^3\Pi_u$ state at high E/n by Taniguchi *et al.* and by Tagashira *et al.* are much lower than ours for $E/n \geq 200$ Td.

VI. DISCUSSION

The results of this paper show that when the electron Boltzmann equation is solved using realistic approximations to the differential cross sections for electron scattering by N_2 the transport and reaction coefficients for moderate and low E/n (< 500 Td) differ by less than 2% from those in which the inelastic scattering is assumed isotropic and the elastic momentum transfer or diffusion cross section is unchanged. At high E/n (> 500 Td) the importance of anisotropic scattering increases with E/n. We have shown that for most transport and reaction coefficients it is more important to allow for the anisotropy of the electron energy distribution beyond the dipole term than to include anisotropic scattering. For the analysis of precision measurements it is necessary to include anisotropic scattering and to use more than two-terms in the spherical-harmonic expansion of the electron energy distribution. Also of considerable importance at high E/n are the corrections to the transport and reaction coefficients arising from the combined effects of electron-density gradients and ionization. In the course of this work we have improved the set of collision cross sections for N_2 at high energies and, through the inclusion of resonance rotational excitation, at low energies.

In this paper we have followed the lead of Blevin[15] by minimizing the number of transport and reaction coefficients calculated for comparison with experiment. We have also attempted to maintain a clear distinction between coefficients calculated using various approximations to the Boltzmann equation and coefficients derived from experimental data. Thus, application of the density gradient expansion to the Boltzmann equation in the hydrodynamic limit yields a rate equation for the electron density and a differential equation for each of what we have called the density gradient expansion transport and reaction coefficients. Appropriate solutions of the rate equation for the electron density can be used to analyze experiments performed using time-of-flight techniques or current growth experiments in time or space. The transport coefficients determined from analyses of these experiments are labeled by the experimental technique and can be compared with the calculated density gradient expansion coefficients. For the analysis of parallel-plane, steady-state, or time-integrated experiments the assumption of an exponential spatial dependence for the electron energy distribution and the electron density reduces significantly the number of velocity-dependent differential equations to be solved. The hydrodynamic spatial growth constant obtained from the solution of this equation can be compared directly with that obtained from experiment. The spatial growth constant can be also calculated from the density gradient expansion transport coefficients when the growth constant is small enough.

There is satisfactory to good agreement between calculated and measured transport coefficients for E/n less than about 100 Td. At higher E/n the difference between calculations and experiment become large, e.g., 30%. At the present time it is not clear whether the source of the discrepancy is in the approximations we used in solving the Boltzmann equation, in the cross section set, or in the

experimental data. From the theoretical side it is important that better techniques be developed for predicting the behavior of electrons at higher E/n where departures from the hydrodynamic model become important. Techniques discussed in the present paper are limited to those for solution of the Boltzmann equation when perturbations caused by spatial gradients are small or when the spatial or temporal gradients can be expressed as an exponential growth. It is important to define the range of validity of these techniques by solving the Boltzmann equation without restrictions as to the variation in space or time. At present such solutions are usually obtained by the Monte Carlo simulation method,[8,9,54] although a few authors[61] have discussed other approaches. Such techniques would also be useful in the treatment of problems where the initial conditions or boundary conditions exert a large influence on the solution, e.g., the backscattering or injected electrons at moderate and low E/n.

The extrapolation of the present results to other gases is difficult because of our lack of knowledge of the range of anisotropic scattering parameters. For example, for H_2 it appears[14] that anisotropic scattering effects are small at low and moderate E/n, but that they may well be larger than for N_2 at high E/n because of indications[25,62] of greater anisotropy and a more rapid decrease in $Q_m(\epsilon)$ with ϵ at high electron energies for H_2 than for N_2. Anisotropic scattering at low energies and low E/n may well be of considerable importance in gases, such as H_2O and other polar gases, where the highly anisotropic inelastic rotational excitation cross section is dominant.[63]

Note Added in Proof. G. N. Haddad [Aust. J. Phys. 37, 487 (1984)] has analyzed electron transport data in N_2-Ar mixtures and in pure N_2. He finds consistency between experimental and calculated transport coefficients by multiplying Schulz's[32] vibrational excitation cross sections by a factor of 1.4, which agrees with our lower value of 1.5 to within our uncertainty.

ACKNOWLEDGMENTS

The authors would like to acknowledge helpful discussions and information regarding the differential-cross-section data and theory from D. C. Cartwright, E. S. Chang, J. Siegel, and especially A. Temkin. They would also like to acknowledge helpful discussions with H. A. Blevin, T. A. Green, P. Segur, and S. S. Yu. The work of A.V.P. was supported in part by the U. S. Army Research Office. The work of L.C.P. was supported by the U. S. Department of Energy.

APPENDIX A: MOMENTUM-TRANSFER CROSS SECTION

Two different definitions of momentum-transfer cross section arise from two different approaches to the solution of the Boltzmann equation. For both the spherical-harmonic and the velocity-moment approaches[64] the momentum-transfer cross section for elastic scattering of electrons is given by Eq. (25). For inelastic scattering the spherical-harmonic technique leads to a definition implicit in Eqs. (21) and (28), i.e.,

$$Q_m^k(\epsilon)=Q_0^k(\epsilon)-(\epsilon+\epsilon_k)Q_1^k(\epsilon+\epsilon_k)f_1(\epsilon+\epsilon_k)/\epsilon f_1(\epsilon)\ . \tag{A1}$$

As was discussed in III, at moderate E/n, the ratio of the distribution functions is often small enough so that the second term in Eq. (A1) can be neglected and $Q_m^k(\epsilon)$ equals its upper limit, i.e., $Q_m^k(\epsilon)=Q_0^k(\epsilon)$. A lower limit to Q_m^k is obtained by assuming that $(\epsilon+\epsilon_k)f_1(\epsilon+\epsilon_k)=\epsilon f_1(\epsilon)$, as is approximately true at E/n and high ϵ. At these high electron energies, where the cross sections for the allowed excitation processes are dominant and the Born approximation is valid, an approximate expression for this limiting value is

$$Q_m^k(\epsilon)\,|_{\min}\approx 3\pi a_0^2\frac{\mathscr{R}\epsilon_i}{\epsilon^2}\left|\frac{z_{0n}}{a_0}\right|^2, \tag{A2}$$

where a_0 and $\mathscr{R}$ are the Bohr radius and the Rydberg, ϵ_i is the ionization energy, and $|z_{0n}|$ is the dipole-matrix element. Here we have used the approximations of Ref. 65, p. 140 in order to obtain a simple closed form. We find the magnitude of Q_m^k in Eq. (A2) to be a sensitive function of the approximations made. Equation (A2) shows that the lower limit to $Q_m^k(\epsilon)$ behaves like elastic scattering at high energies. See Strickland *et al.*[24] Note that the transition between the limiting forms of $Q_m^k(\epsilon)$ discussed here is automatically included in the multiterm Boltzmann code used in this paper when anisotropic inelastic scattering is considered.

The velocity moment method of solving the Boltzmann equation[64] leads to a second definition of the momentum-transfer cross section for inelastic collisions which is sometimes cited in the literature.[66] According to this procedure the contribution of the kth inelastic process to the momentum equation, e.g., Eq. (2-38b) of Ref. 64, can be written as

$$\begin{aligned}\int v\cos\theta C[F(\mathbf{v})]d^3v\,|_k &= -\frac{8\pi^2}{m}\int_0^\pi\left[\int_{\epsilon_k}^\infty \epsilon^{3/2}I^k(\epsilon,\theta_s)F(\epsilon,\theta)d\epsilon\right]\cos\theta\sin\theta_s\,d\theta_s \\ &\quad+\frac{8\pi^2}{m}\int_0^\pi\left[\int_0^\pi(\epsilon+\epsilon_k)I^k(\epsilon+\epsilon_k,\theta_s)F(\epsilon+\epsilon_k,\theta)\epsilon^{1/2}d\epsilon\right]\cos\theta\sin\theta'\,d\theta' \\ &= -\frac{4\pi}{m}\int_0^\pi\left[\int_{\epsilon_k}^\infty \epsilon^{3/2}\mathscr{Q}_m^k(\epsilon)F(\epsilon,\theta)d\epsilon\right]\cos\theta\sin\theta\,d\theta\ ,\end{aligned} \tag{A3}$$

where θ and θ_s are the polar angles measured from the direction of acceleration and the direction of the incident electron, respectively; $\theta'=\theta-\theta_s$; and

$$\mathscr{Q}_m^k(\epsilon)=Q_0^k(\epsilon)-\left[\frac{(\epsilon-\epsilon_k)}{\epsilon}\right]^{1/2}Q_1^k(\epsilon)\ . \tag{A4}$$

The square-root factor in Eq. (A4) is particularly important near the excitation threshold. Applying the simplified Born approximation used in Eq. (A2), $\mathscr{Q}_m^k$ at high energies is given by

$$\mathscr{Q}_m^k(\epsilon)\approx 2\pi a_0^2\frac{\mathscr{R}\epsilon_i}{\epsilon^2}\left|\frac{z_{0n}}{a_0}\right|^2\ln\left[\frac{4\epsilon}{\epsilon_k}\right]\ . \tag{A5}$$

As the electron energy increases $\mathscr{Q}_m^k$ becomes significantly larger than Q_m^k. In the high ϵ limit $\sum\mathscr{Q}_m^k\approx L(\epsilon)/2\epsilon$. Here $L(\epsilon)$ is the energy-loss function used in the continuous-slowing-down treatments of electron energy degradation in gases[23,43,51] and in models of runaway electrons.[67] Of course elastic scattering must be added to Eqs. (A3)—(A5) to obtain the full momentum loss.

One way to reduce the confusion resulting from the dual definition of the momentum-transfer cross section is to adopt the terminology of diffusion cross section[65] for the cross sections of Eq. (A1). This choice is made since the cross section defined by Eq. (A4) more accurately represents the momentum loss caused by inelastic collisions. Note that since $Q_m^0=\mathscr{Q}_m^0$ there is no confusion for elastic collisions.

APPENDIX B: RESONANCE ROTATIONAL EXCITATION

In this appendix we analyze measurements of the heating of N_2 by low-energy electrons and obtain an effective cross section for resonance rotational excitation of N_2. Figure 11 shows the calculated values (smooth curves) and measured values (points) of the fractional energy input to gas heating versus E/n. In this calculation we assume that gas heating occurs as the result of the rapid relaxation to the gas temperature of rotationally and electronically excited states. We assume that, while vibrational excitation may be redistributed within the vibrational manifold, vibrational relaxation to translational energy is too slow to change the gas temperature on the time scale of the experiments. The experiments shown for E/n below about 35 Td involved measurements of the increase in temperature of the flowing gas during a known excitation time.[68] The experiments shown for $E/n>40$ Td were carried out in the positive column of a steady-state glow discharge[69] in which the degree of vibrational relaxation is unknown. The solid curve was calculated using the cross section set discussed in Sec. III and using the two-term spherical-harmonic expansion with isotropic inelastic scattering. Rotational excitation is the dominant source of gas heating for E/n below 40 Td. The shape of the rotational excitation cross section used is based on the sum of the vibrational excitation cross sections of Sec. III B, the threshold is chosen as outlined in Ref. 70, and the magnitude is adjusted to fit the experimental data of Fig. 11 for E/n below 40 Td.

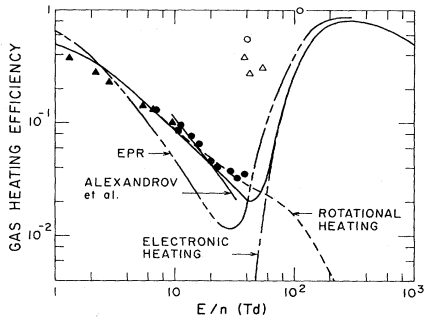

FIG. 11. Short-time heating efficiency for electrons in N_2 versus E/n. The solid curve is the result of our fitting the resonant rotational excitation to the experimental points. Symbols, authors, and references are the following: ■, Culick *et al.* (Ref. 68); ●, Napartovich *et al.* (Ref. 68); △, Londer *et al.* (Ref. 68); ○, Kosoruchkina (Ref. 69); ▲, Krymanski and Walter (Ref. 69).

For E/n between 20 and 80 Td there is a significant correction to the calculated gas heating because of gas cooling or heating during the process of anharmonic vibrational relaxation to the vibrational temperature.[71,72] The net anharmonic heating H for molecules initially in the ground vibrational levels is given by

$$H=\frac{\omega_e x_e}{W(E/n)}\left[-\sum_{v=1}^{\infty}v^2k(v)+\frac{\sum_{v=1}^{\infty}v^2p(v)}{\sum_{v=1}^{\infty}vp(v)}\sum_{v=1}^{\infty}vk(v)\right]\ . \tag{B1}$$

where ω_e and x_e are the vibrational constant and anharmonic constant for ground state N_2, $k(v)$ is the excitation rate coefficient for vibrational level v, and $p(v)$ is the final probability distribution for the vibrational levels. For our assumed low final vibrational temperature of ≤ 500 K the ratio

$$\sum_{v=1}^{\infty}v^2p(v)\Big/\sum_{v=1}^{\infty}vp(v)$$

equals 1 and the effect of anharmonic relaxation is to cool the N_2. This cooling is indicated by the fact that for E/n below 50 Td the final result (solid curve) is below that for heating by rotational excitation (short dashes). If the energy stored in vibration were as high as in recent discharge models,[73] then this ratio might be as large as 20 and gas heating by vibrational redistribution would raise the minimum of the solid curve of Fig. 11 to about 12%.

The curve marked EPR is the sum of the calculated direct rotational excitation and electronic excitation calculated by Engelhart *et al.*,[22] since their analysis did not include resonance rotational excitation. The short solid line is obtained from calculations by Alexandrov *et al.*[74] which included resonant rotational excitation cross sections from Oksyuk.[30]

For E/n above 40 Td there is poor agreement between

this model and the experimental measurements. A number of attempts[75] have been made to explain positive-column temperature-rise data. Some of the factors considered include gas heating by anharmonic relaxation to a high vibrational temperature, increases in the rate coefficients for electronic excitation with changes in the electron energy distribution in the presence of vibrationally excited N_2, and collisions among excited N_2 molecules.

---

*Quantum Physics Division, National Bureau of Standards and Department of Physics, University of Colorado.

†Current address: GTE Laboratories, Inc., Waltham, MA 02254.

[1]L. C. Pitchford, S. V. ONeil, and J. R. Rumble, Jr., Phys. Rev. A **23**, 294 (1981).

[2]L. C. Pitchford and A. V. Phelps, Phys. Rev. A **25**, 540 (1982). R. W. Crompton points out that r in Eqs. (2) and (3) should be replaced by $\rho = |\mathbf{r}| \sin\theta$ and that $g_r(\mathbf{v})$ should be replaced by $g_\rho(\mathbf{v})$ in Eqs. (2)—(18). Here $\mathbf{r}$ remains unchanged. J. P. Novak points out that the units of w in Table I should be 10^4 m sec^{-1}. Also, the left-hand side of Eq. (24) should be multiplied by N and the first factor on the right-hand side of the equation for w^{II} after Eq. (23) should be $eE/3N$. The last two terms in Eq. (19) should be multiplied by j and $j+1$, respectively.

[3]S. Yoshida, A. V. Phelps, and L. C. Pitchford, Phys. Rev. A **27**, 2858 (1983).

[4]I. D. Reid, Aust. J. Phys. **32**, 231 (1979).

[5]G. N. Haddad, S. L. Lin, and R. E. Robson, Aust. J. Phys. **34**, 243 (1981).

[6]L. C. Pitchford and A. V. Phelps, Bull. Am. Phys. Soc. **27**, 109 (1982).

[7]M. A. Folkhard and S. C. Haydon, J. Phys. B **6**, 214 (1973).

[8]Y. Tzeng and E. E. Kunhardt, Bull. Am. Phys. Soc. **28**, 180 (1983).

[9]H. N. Kücükarpaci and J. Lucas, J. Phys. D **12**, 2123 (1979); E. E. Kunhardt and Y. Tzeng (unpublished). Note the Kücükarpaci and Lucas find it necessary to reduce the vibrational excitation cross sections of Ref. 22 by a factor of 0.3. The use of such low cross sections in our calculation gives a very poor fit to experiment, e.g., a factor of about 4 error in the energy-exchange frequency of Ref. 22 for mean electron energies near 1 eV.

[10]J. H. Parker, Jr. and J. J. Lowke, Phys. Rev. **181**, 290 (1969).

[11]H. Tagashira, Y. Sakai, and S. Sakamoto, J. Phys. D **10**, 1051 (1977).

[12]K. Kumar, H. R. Skullerud, and R. E. Robson, Aust. J. Phys. **33**, 343 (1980).

[13]L. G. H. Huxley and R. W. Crompton, *The Diffusion and Drift of Electrons in Gases* (Wiley, New York, 1974), Chap. 2.

[14]H. A. Blevin, J. Fletcher, and S. R. Hunter, J. Phys. D **9**, 1671 (1976); **11**, 1653 (1978); J. Fletcher, in *Electron and Ion Swarms,* edited by L. G. Christophorou (Pergamon, Oxford, 1981), p. 1.

[15]H. A. Blevin, J. Fletcher, and L. M. Marzec, J. Phys. D **9**, 465 (1976); H. A. Blevin, in Abstracts of Papers for the Third Gaseous Electronics Meeting, Canberra, 1984 (unpublished), p. 18; H. A. Blevin and J. Fletcher Aust. J. Phys. **37**, 593 (1984).

[16]Consider the form of this technique described by L. Frommhold, Z. Phys. **156**, 144 (1959). During the current growth portion of the waveform the voltage is given by $(Q_0/C)\exp(vt)$, where Q_0 is the charge released from the cathode and C is the circuit capacity. After the electrons and ions have been collected the voltage is given by $(Q_0/C)\exp(\alpha_i d)$. From the time of intersection of these curves we find $d/t = v/\alpha_i = V_p$.

[17]D. Levron and A. V. Phelps, Bull. Am. Phys. Soc. **24**, 129 (1979).

[18]W. Legler, Z. Phys. **173**, 169 (1963); K. Tachibana and A. V. Phelps, J. Chem. Phys. **71**, 3544 (1979); V. V. Urošević, J. V. Božin, and Z. Lj. Petrovic, Z. Phys. A **309**, 293 (1983).

[19]W. R. L. Thomas, J. Phys. B **2**, 551 (1969); H. Brunet and P. Vincent, J. Appl. Phys. **50**, 4700 (1979); **50**, 4708 (1979); J. P. Novak and M. F. Fréchette, *ibid.* **55**, 107 (1984).

[20]T. Holstein, Phys. Rev. **70**, 367 (1946); W. P. Allis, Handb. Phys. **21**, 383 (1956); L. S. Frost and A. V. Phelps, Phys. Rev. **127**, 1621 (1962).

[21]A. V. Phelps and L. C. Pitchford, Joint Institute for Laboratory Astrophysics Information Center Report No. 26 (unpublished).

[22]A. G. Englehardt, A. V. Phelps, and C. G. Risk, Phys. Rev. **135**, A1566 (1964).

[23]J. P. Bromberg, J. Chem. Phys. **50**, 3906 (1969); T. G. Finn and J. P. Doering, *ibid.* **63**, 4399 (1975); S. K. Srivastava, A. Chutjian, and S. Trajmar, *ibid.* **64**, 1340 (1976); R. H. J. Jansen, F. J. de Heer, H. J. Luyken, B. van Wingerden, and H. J. Blaauw, J. Phys. B **9**, 185 (1976); T. W. Shyn and G. R. Carignan, Phys. Rev. A **22**, 923 (1980). Note that the value from Bromberg has been reinterpreted as discussed by Finn and Doering.

[24]M. E. Riley, C. J. MacCallum, and F. Biggs, At. Data. Nucl. Data Tables **15**, 443 (1975); D. J. Strickland, D. L. Book, T. P. Coffey, and J. A. Fedder, J. Geophys. Res. **81**, 2755 (1976). The magnitudes of the spherical-harmonic components of the screened Coulomb cross sections were calculated using formulas given by M. J. Berger, in *Methods in Computational Physics,* edited by B. Alder, S. Fernbach, and M. Rotenberg (Academic, New York, 1963), p. 209. As suggested by these references, our comparisons of experiment and theory suggest screening lengths of 0.015 at 500 eV and 0.01 at 1 keV.

[25]M. Hayashi, Nagoya Institute of Technology Report No. IPPJ-AM-19, 1981 (unpublished).

[26]T. Taniguchi, H. Tagashira, and Y. Sakai, J. Phys. D **11**, 1757 (1978); H. Tagashira, T. Taniguchi, and Y. Sakai, *ibid.* D **13**, 235 (1980).

[27]S. Pfau and W. Winkler, Beitr. Plasmaphys. **18**, 113 (1978).

[28]R. D. DuBois and M. E. Rudd, J. Phys. B **9**, 2657 (1976); R. D. DuBois (private communication).

[29]N. Chandra and A. Temkin, Phys. Rev. A **13**, 188 (1976); *ibid.* **14**, 507 (1976); U. S. National Aeronautics and Space Administration Technical Note No. TN-D-8347, 1976 (unpublished); J. Siegel, J. L. Dehmer, and D. Dill, Phys. Rev. A **21**, 85 (1980); J. Siegel and J. L. Dehmer (private communication).

[30]J. Comer and M. Harrison, J. Phys. B **6**, L70 (1973); F. H. Read and D. Andrick, *ibid.* **4**, 911 (1971); S. F. Wong and L. Dubé, Phys. Rev. A **17**, 570 (1978); K. Jung, Th. Antoni, R. Müller, K.-H. Kochem, and H. Ehrhardt, J. Phys. B **15**, 3535 (1982).

[31]Yu. D. Oksyuk, Zh. Eksp. Teor. Fiz. **49**, 1261 (1965) [Sov. Phys.—JETP **22**, 873 (1966)]; P. G. Burke and A.-L. Sinfailam, J. Phys. B **3**, 641 (1970); N. Chandra and P. G. Burke,

ibid. **6**, 2355 (1973); B. D. Buckley and P. G. Burke, *ibid.* **10**, 725 (1977); E. S. Chang, *ibid.* **15**, L873 (1982).

[32]G. J. Schulz, Phys. Rev. **135**, A988 (1964).

[33]D. Spence, J. L. Mauer, and G. J. Schulz, J. Chem. Phys. **57**, 5516 (1972).

[34]L. J. Kieffer, Joint Insitute for Laboratory Astrophysics Information Center Report No. 13, 1973 (unpublished). The data tabulated in this report were modified to give a common energy grid for all levels while preserving the areas under the peaks in the cross sections.

[35]G. J. Schulz, Phys. Rev. **125**, 229 (1962).

[36]Z. Pavlović, M. J. W. Boness, A. Herzberg, and G. J. Schulz, Phys. Rev. **6**, 676 (1972); D. G. Truhlar, M. A. Brandt, S. K. Srivastava, S. Trajmar, and A. Chutjian, J. Chem. Phys. **66**, 655 (1977).

[37]L. S. Polak and D. I. Slovetskii, Teplofiz. Vys. Temp. **10**, 645 (1972) [High Temperature (USSR) **10**, 575 (1972)]; see also, G. J. Schulz, Rev. Mod. Phys. **45**, 423 (1973).

[38]D. C. Cartwright, S. Trajmar, A. Chutjian, and W. Williams, Phys. Rev. A **16**, 1041 (1977). Revisions of the data of this reference and of Refs. 44 and 47 are given in S. Trajmar, D. F. Register, and A. Chutjian, Phys. Rep. **97**, 219 (1983). For our purposes these changes are small and will be neglected.

[39]A. Lofthus and R. H. Krupenie, J. Phys. Chem. Ref. Data **6**, 113 (1977).

[40]J. Olmsted III, A. S. Newton, and K. Street, Jr., J. Chem. Phys. **42**, 2321 (1965); W. L. Borst, Phys. Rev. A **5**, 648 (1972). For recent results and discussion of previous work, see J. N. H. Brunt, G. C. King, and F. H. Read, J. Phys. B **11**, 173 (1978).

[41]D. E. Shemansky and A. L. Broadfoot, J. Quant. Spectrosc. Radiat. Transfer **11**, 1401 (1971); T. G. Finn, J. F. M. Arts, and J. P. Doering, J. Chem. Phys. **56**, 5632 (1972); E. Kisker, Z. Phys. **257**, 51 (1972); M. Imani and W. L. Borst, J. Chem. Phys. **61**, 1115 (1974); D. E. Golden, D. J. Burns, and V. C. Sutcliffe, Jr., Phys. Rev. A **10**, 2123 (1974).

[42]W. L. Borst, W. C. Wells, and E. C. Zipf, Phys. Rev. A **5**, 1744 (1972).

[43]E. C. Zipf and R. W. McLaughlin, Planet. Space Sci. **26**, 449 (1978).

[44]C. H. Jackman, R. H. Garvey, and A. E. S. Green, J. Geophys. Res. **82**, 5081 (1977).

[45]A. Chutjian, D. C. Cartwright, and S. Trajmar, Phys. Rev. A **16**, 1052 (1977).

[46]D. Rapp and P. Englander-Golden, J. Chem. Phys. **43**, 1464 (1965); B. L. Schramm, F. J. de Heer, M. J. van der Wiel, and J. Kistemaker, Physica (Utrecht) **31**, 94 (1965). The cross-section values actually used are from C. F. Barnet, J. A. Ray, E. Ricci, M. I. Wilker, E. W. McDaniel, E. W. Thomas, and H. B. Gilbody, Oak Ridge National Laboratory Report No. 5207, 1977 (unpublished).

[47]C. B. Opal, W. K. Peterson, and E. C. Beaty, J. Chem. Phys. **55**, 4100 (1971); C. B. Opal, E. C. Beaty, and W. K. Peterson, At. Data Nucl. Data Tables **4**, 209 (1972); R. D. DuBois and M. E. Rudd, Phys. Rev. A **17**, 843 (1978).

[48]D. C. Cartwright, A. Chutjian, S. Trajmar, and W. Williams, Phys. Rev. A **16**, 1013 (1977).

[49]S. M. Silverman and E. N. Lassettre, J. Chem. Phys. **42**, 3420 (1965); A. Skerbele and E. N. Lassettre *ibid.* **53**, 3806 (1970).

[50]It should be kept in mind that the differential scattering cross sections reconstructed from our limited number of spherical harmonics will not give a good representation of a sharply peaked angular distribution at small scattering angles and may become negative at some large angles.

[51]S. Chung and C. C. Lin, Phys. Rev. A **6**, 988 (1972); A. W. Fliflet, V. McKoy, and T. N. Rescigno, J. Phys. B **12**, 3281 (1979); T. K. Holley, S. Chung, C. C. Lin, and E. T. P. Lee, Phys. Rev. A **24**, 2946 (1981); L. Mu-Tao and V. McKoy, *ibid.* **28**, 697 (1983).

[52]C. H. Jackman and A. E. S. Green, J. Geophys. Res. **84**, 2715 (1979); J. Wilhelm and R. Winkler, Ann. Phys. (N.Y.) **36**, 333 (1979).

[53]H. J. Blaauw, R. W. Wagenaar, D. H. Barends, and F. J. de Heer, J. Phys. B **13**, 359 (1980); R. E. Kennerly, Phys. Rev. A **21**, 1876 (1980); G. Dalba, P. Fornasini, R. Grisenti, G. Ranieri, and A Zecca, J. Phys. B **13**, 4695 (1980); K. R. Hoffman, M. S. Dababneh, Y.-F. Hsieh, W. E, Kauppila, V. Pol, J. H. Smart, and T. S. Stein, Phys. Rev. A **25**, 1393 (1982).

[54]G. L. Braglia, L. Romanò, and M. Diligenti, Phys. Rev. A **26**, 3689 (1982); Lett. Nuovo Cimento **35**, 193 (1982); see also B. M. Penetrante, J. N. Bardsley, and L. C. Pitchford (unpublished).

[55]J. J. Lowke, Aust. J. Phys. **16**, 115 (1963); H. Schlumbohm, Z. Phys. **184**, 492 (1965); J. Fletcher and I. D. Reid, J. Phys. D **13**, 2275 (1980).

[56]R. W. Crompton and D. J. Sutton, Proc. R. Soc. (London) Ser. A **215**, 467 (1952); R. W. Warren and J. H. Parker, Jr., Phys. Rev. **128**, 2661 (1962); N. Kontoleon, J. Lucas and L. E. Virr, J. Phys. D **6**, 1237 (1973); W. Roznerski and K. Lega, *ibid.* **13**, L181 (1980).

[57]L. Frommhold, Z. Phys. **160**, 554 (1960); U. Dibbern, *ibid.* **163**, 582 (1961); P. Felsenthal and J. M. Proud, Phys. Rev. **139**, A1796 (1965); W. W. Byszewski, M. J. Enright, and J. M. Proud, IEEE Trans. Plasma Sci. **PS-10**, 281 (1982).

[58]A. Buffa, G. Malesani, and G. F. Nalesso, Phys. Rev. A **3**, 955 (1971); T. Fujiwara, T. Shimada, and K. Sugita, J. Phys. D **16**, 1217 (1983).

[59]S. C. Haydon and O. M. Williams, J. Phys. D **9**, 523 (1976).

[60]See comment in the title of Fig. 2.6 of G. J. Schulz, in *Principles of Laser Plasmas,* edited by G. Bekefi (Wiley, New York, 1976), p. 47; see also, Jung *et al.* (Ref. 30).

[61]For a recent review, see, P. Segur, M. Yousfi, J. P. Bouef, E. Marode, A. J. Davies, and J. G. Evans, in *Electrical Breakdown and Discharges in Gases,* edited by E. E. Kunhardt and L. H. Luessen (Plenum, New York, 1981), p. 331.

[62]J. Fletcher and S. C. Haydon, Aust. J. Phys. **19**, 615 (1966); G. Csanak, D. C. Cartwright, S. K. Srivastava, and S. Trajmar, in *Electron-Molecule Interactions and Their Applications,* edited by L. G. Christophorou (Academic, New York, 1983), Chap. 1.

[63]D. Norcross and L. A. Collins, in *Advances in Atomic and Molecular Physics,* edited by D. R. Bates and B. Bederson (Academic, New York, 1982), Vol. 18, p. 341.

[64]I. P. Shkarofsky, T. W. Johnston, and M. P. Bachynski, *The Particle Kinetics of Plasmas* (Addison-Wesley, Reading, Mass., 1966), p. 57.

[65]H. S. W. Massey and E. H. S. Burhop, *Electronic and Ionic Impact Phenomena* (Oxford, London, 1952), pp. 14 and 140.

[66]See, for example, G. Ecker and K. G. Muller, Z. Naturforsch. **16a**, 246 (1961); A. Altschuler, J. Geophys. Res. **68**, 4707 (1963); F. J. McCormack Phys. Rev. **178**, 319 (1969); D. C. Cartwright, J. Appl. Phys. **49**, 3855 (1978). It appears to us that the procedure of Lin, Robson, and Mason does not belong in this category, since they made the spherical-harmonic expansion before making the velocity-moment expansion. See, S. L. Lin, R. E. Robson, and E. A. Mason, J. Chem. Phys. **71**, 3483 (1979).

[67]A. V. Gurevich, Zh. Eksp. Teor. Fiz. **39**, 1296 (1960) [Sov.

Phys.—JETP **12**, 309 (1961)].

[68]F. E. C. Culick, P. I. Shen, and W. S. Griffin, IEEE, J. Quantum. Electron. **QE-12**, 566 (1976); A. P. Napartovich, V. G. Naumov, and V. M. Shashov, Dokl. Akad. Nauk SSSR **232**, 570 (1977) [Sov. Phys. Dokl. **22**, 35 (1977)]; Ya. I. Londer, L. P. Menakhin, G. L. Popova, and K. N. Ul'yanov, Zh. Tekh. Fiz. **49**, 2490 (1979) [Sov. Phys.—Tech. Phys. **49**, 1407 (1979)].

[69]A. D. Kosoruchkina, Zh. Tekh. Fiz. **45**, 1077 (1975) [Sov. Phys.—Tech. Phys. **20**, 676 (1975)]; K. H. Krysmanski and W. Walter, Beitr. Plasmaphys. **18**, 367 (1978).

[70]The single-level approximation is discussed by R. D. Hake and A. V. Phelps, Phys. Rev. **158**, 70 (1967).

[71]B. R. Bulos and A. V. Phelps, Phys. Rev. A **14**, 615 (1976). For earlier work on vibrational cooling in air, see, for example, A. D. Wood, M. Camac, and E. T. Gerry, Appl. Opt. **10**, 1877 (1971).

[72]V. Yu. Baranov, F. I. Vysiklailo, A. P. Napartovich, V. G. Niz'ev, S. V. Pigul'skii, and A. N. Starostin, Fiz. Plazmy **4**, 358 (1978) [Sov. J. Plasma Phys. **4**, 201 (1978)]. When the distribution of vibrationally excited molecules produced during the excitation period is used instead of the rate coefficients in Eq. (B1), we obtain the equivalent of the equation given in this reference.

[73]M. Capitelli and M. Dilonardo, Rev. Phys. Appl. **13**, 115 (1978); M. Capitelli, M. Dilonardo, and C. Gorse, Chem. Phys. **56**, 29 (1981).

[74]N. L. Alexandrov, A. M. Konchakov, and É. E. Son, Fiz. Plazmy **4**, 169 (1978) [Sov. J. Plasma Phys. **4**, 98 (1978)].

[75]Yu. S. Akishev, A. V. Dem'yanov, I. V. Kochetov, A. P. Napartovich, S. V. Pashkin, V. V. Ponomarenko, V. G. Pevgov, and V. B. Podobedov, Teplofiz. Vys. Temp. **20**, 818 (1982) [High Temp. **20**, 658 (1982)]; J. P. Boeuf and E. E. Kunhardt, Bull. Am. Phys. Soc. **28**, 188 (1983).